nature communications

Article

https://doi.org/10.1038/s41467-026-70663-1

A dihydrouracil CRBN ligand mitigates IMiD associated safety liabilities in heterobifunctional targeted protein degrader

Received: 6 December 2024

Accepted: 25 February 2026

Published online: 25 March 2026

Check for updates

Monica C. Rodrigo-Brenni[1], Jasper C. Komen[1], Ghaith M. Hamza[2], Natacha Bohin[1], Tomas Adomavicius[3], Angelo Andres[2], Stefan Blaho[4], Ulf Börjesson[5], Gavin W. Collie[3], Gian Marco De Donatis[6], Frederik Eisele[7], Ning Gao[2], Andrea Gohlke[3], Christoph Grebner[5], Frida Gustafsson[1], Andreas Hock[6], Cecilia Kankkonen[7], Praveen Kumar[8], Emilyanne Leonard[9], Xin Li[10], Ruth Macdonald[11], Katja Madeyski-Bengtson[12], Eric Miele[2], Philip Nevin[7], Jeroen Overman[6], Fiona Pachl[2], Claudio Pathe[6], Matthew W. D. Perry[13], Christopher Phillips[3], Andy Pike[14], Ian Purvis[11], Timothy Rasmusson[2], Sophie Regan[1], Linda Reilly[1], Jonathan Rose[11], R. Ian Storer[15], Jingwen Wang[10], Xiang Zhai[2], Iacovos N. Michaelides[15] ✉ & Kevin Moreau[1] ✉

Immunomodulatory imide drugs (IMiDs) like lenalidomide and pomalidomide are effective in treating multiple myeloma (MM) but pose hematotoxicity risks by degrading neosubstrates Ikaros (IKZF1) and Aiolos (IKZF3). When these IMiD scaffolds are integrated into proteolysis targeting chimeras (PROTACs), they can inadvertently lead to the degradation of these neosubstrates alongside the intended protein of interest (POI), raising safety concerns. This study profiles existing PROTACs and reveals instances of undesired degradation of IMiD-associated neosubstrates. We have developed in vitro hematopoietic assays to scrutinize the IMiD effects and describe the mechanistic insights on cell differentiation rewiring towards megakaryocytes together with an activation of the interferon response that is phenocopied by an Ikaros knock-out model. Moreover, we have identified a CRBN ligand that mitigates these safety liabilities and can be effectively incorporated into PROTACs. This advancement provides a promising path toward safer preclinical development of PROTACs, especially as the field expands into chronic disease treatments beyond oncology.

The immunomodulatory imide drug (IMiD) thalidomide has profoundly transformed drug discovery, especially with respect to the safety profiling of molecules before entering the clinic. Initially launched in multiple countries to treat morning sickness in pregnant women, thalidomide caused more than 10,000 children to be born with severe birth defects such as phocomelia, as well as thousands of miscarriages[1,2]. Interestingly, thalidomide was later repurposed and shown to be efficacious in the treatment of multiple myeloma (MM) with the related IMiDs lenalidomide and pomalidomide now being the standard of care in this disease[3].

A full list of affiliations appears at the end of the paper. ✉e-mail: iacovos.michaelides@astrazeneca.com; kevin.moreau@astrazeneca.com

It took 50 years to identify the mechanisms behind thalidomide's developmental toxicities and the multiple myeloma clinical activity. The teratogenic effects are the result of the degradation of several transcription factors (TFs), including SALL4, critical for embryogenesis[4–8]. Beyond SALL4, IMiDs degrade TFs such as Ikaros and Aiolos, in part responsible for the drugs' efficacy in the treatment of multiple myeloma through a molecular glue (MG) mechanism of action (MoA)[9–11]. IMiDs bind to the E3 ubiquitin ligase cereblon (CRBN), inducing the recruitment of proteins called neosubstrates to the E3 ligase complex and resulting in their ubiquitination and degradation by the proteasome. This MoA has since energised the targeted protein degradation (TPD) field, with numerous MG degraders entering the clinic[12,13].

The binding of IMiDs to CRBN has led to the repurposing of these molecules within the proteolysis targeting chimera (PROTAC) modality. Unlike the monovalent MG degraders, PROTACs are heterobifunctional molecules formed by the attachment of an E3 ligase ligand to a protein of interest (POI) ligand. There are more than 20 PROTACs in clinical trials, with the most advanced degraders targeting the oestrogen and androgen receptors[13,14]. When assessing the chemical structures of the disclosed PROTACs, it is striking to observe that the vast majority are designed to recruit CRBN[15]. CRBN is a ligandable E3 ligase and ligands like the IMiDs have properties that lend themselves to the design of cell permeable and orally bioavailable PROTACs – the latter properly acknowledged as a challenging aspiration at the advent of this beyond Lipinski "rule of 5"[16] (bRo5) modality[12–15,17–19].

However, by repurposing IMiDs in PROTACs, these then carry the risk of introducing IMiD-associated safety liabilities[20]. SALL4 degradation would likely cause developmental toxicities, while the degradation of Ikaros and Aiolos has been associated with bone-marrow toxicities. It is therefore crucial to assess the likelihood of degrading these off-target neosubstrates when developing IMiD-based PROTACs and understand the potential associated toxicities[20].

In this work, using a high-throughput proteomics workflow, we demonstrate that several previously reported IMiD-based PROTACs degrade neosubstrates such as Ikaros and Aiolos, alongside other unintended targets. We further characterise the consequences of degrading Ikaros on primary human hematopoietic stem and progenitor cells (HSPC). Using our high-throughput proteomics workflow, we provide relevant mechanistic insights into the effect on stem cell differentiation, demonstrating the versatility of our platform to capture both off-target degradation and phenotypic changes for mechanistic understanding. Importantly, we have identified an alternative CRBN ligand to the canonical IMiDs, based on a dihydrouracil (DHU) motif. This ligand can be incorporated into PROTACs, capable of degrading numerous POIs whilst sparing the degradation of the IMiD-neosubstrates. This ligand discovery, coupled with the rigorous in vitro safety cascade described, is expected to pave the way for the design of efficacious, selective and thus safer CRBN-recruiting PROTACs.

Results

IMiD-based heterobifunctional degraders can degrade IMiD neosubstrates

To assess the selectivity of IMiD-based PROTACs, we deployed high-throughput proteomics. Data-independent acquisition parallel accumulation-serial fragmentation (diaPASEF) on the timsTOF flex instrument connected to the Evosep One LC system resulted in efficient and streamlined data acquisition, which was subsequently analyzed by DIA-NN for peak picking and quantification[21,22]. The workflow supports the analysis of 60 samples per day, with ~6000 proteins detected in each sample, allowing for robust profiling of protein modulation (Fig. 1A and Supplementary Fig. 1). We validated the workflow in the leukaemia cell line NB-4 treated in a six-point dose response for 5 h with various IMiDs, or IMiD-related molecules like the GSPT1 degrader CC-885 or the specific casein kinase 1 alpha (CSNK1A1) degrader TMX-4116 (Supplementary Fig. 2)[23,24]. We confirmed the dose-dependent reduction of Ikaros with lenalidomide, pomalidomide and iberdomide as well as their potency ranking (iberdomide > pomalidomide > lenalidomide) (Fig. 1B(i), C and Supplementary Data 1). We also observed the potent reduction of GSPT1 with CC-885 and the anticipated selectivity of the CSNK1A1 degrader TMX-4116 (Fig. 1B(i), C, Supplementary Fig. 2, and Supplementary Data 1). Next, we tested the IMID-based PROTACs, dBRD9 and ZXH-3-26, and confirmed their ability to selectively reduce their respective primary targets, BRD9 and BRD4 (Supplementary Fig. 2 and Supplementary Data 1). In addition to their primary targets, dBRD9 and ZXH-3-26 also reduce Ikaros and Aiolos (Fig. 1B(ii), C). As additional examples, we profiled two IMiD-based PROTACs with different kinase selectivity profiles: the pan-kinase degrader TL12-186[25] and the ALK selective degrader TL13-112[25] (Supplementary Fig. 2). While we confirmed the respective expected kinase selectivity profiles, both showed Ikaros and Aiolos reduction (Fig. 1B(ii), C). Having shown the potential of IMiD-based PROTACs to degrade Ikaros, we focused our study on the biological consequences on primary human hematopoietic stem and progenitor cells (HSPCs).

IMiDs block the proliferation of hematopoietic stem and progenitor cells through Ikaros degradation

Whilst previous studies have linked the hematological toxicities seen in the clinic with IMiDs to Ikaros degradation, no screening strategy has been reported, and the mechanism remains elusive[26–28]. To that end, we assessed the effect of IMiDs on the proliferation of primary HSPCs that give rise to the various lineages of the bone marrow compartment. To confirm the IMiD-driven MG MoA, we used a CRISPR targeting approach to generate a genetic deletion of CRBN (Fig. 2A). After 4 days of gene editing, we confirmed robust depletion of CRBN via immunoblotting (Fig. 2B). We first characterised the effect of IMiDs in mock-treated cells, where expression of CRBN is maintained (Fig. 2B, Mock). Both lenalidomide and pomalidomide treatment led to a reduction of Ikaros, similar to that observed in MM cell lines[9,10]. This degradation was dependent on CRBN, as no degradation was observed upon its knock-out (Fig. 2B, CRBN KO). We measured the levels of ATP in the HSPC, as a surrogate for cell number, over 5 days and observed a decrease when treated with lenalidomide, pomalidomide or iberdomide (Fig. 2C). Interestingly, the reduced cell numbers correlated with the Ikaros degradation potency and was abolished in the CRBN knock-out condition (Supplementary Fig. 3A). To gain confidence in the mechanism behind the IMiD effects in HSPC, we deleted the Ikaros gene using CRISPR (Fig. 2D(i)) and we observed that Ikaros knock-out cells showed a strong reduction in cell numbers (Fig. 2D(ii)). To distinguish between cytotoxicity and proliferation defects, we measured viability via the incorporation of a live/dead dye by flow cytometry. The high viability of the cells, together with the reduced cell numbers, suggests a cytostatic mechanism rather than a cytotoxic one (Fig. 2E). The high viability observed after 5 days of 2D culture was maintained over 13 days in culture, assessed via a 3D static bone-marrow model (Supplementary Fig. 3B), in line with previous literature[29]. Our data also emphasise the need for screening of viability effects associated with CRBN-engaging degraders in relevant cell models.

When assessing the consequences of degrading Ikaros and Aiolos by IMiDs in vivo, the choice of the animal model is critically important[20]. It is now understood that IMiDs are not pharmacologically active in rodents, at least not via the MG MoA, due to a primary sequence difference in CRBN, compared to humans. Strikingly, one amino acid change from valine to isoleucine in the 391 position of the sequence, between human and mouse, respectively, is enough to ablate the IMiD sensitivity in mice[28]. Fink et al. generated a transgenic model to replace the isoleucine with a valine in mouse Crbn, which

https://doi.org/10.1038/s41467-026-70663-1

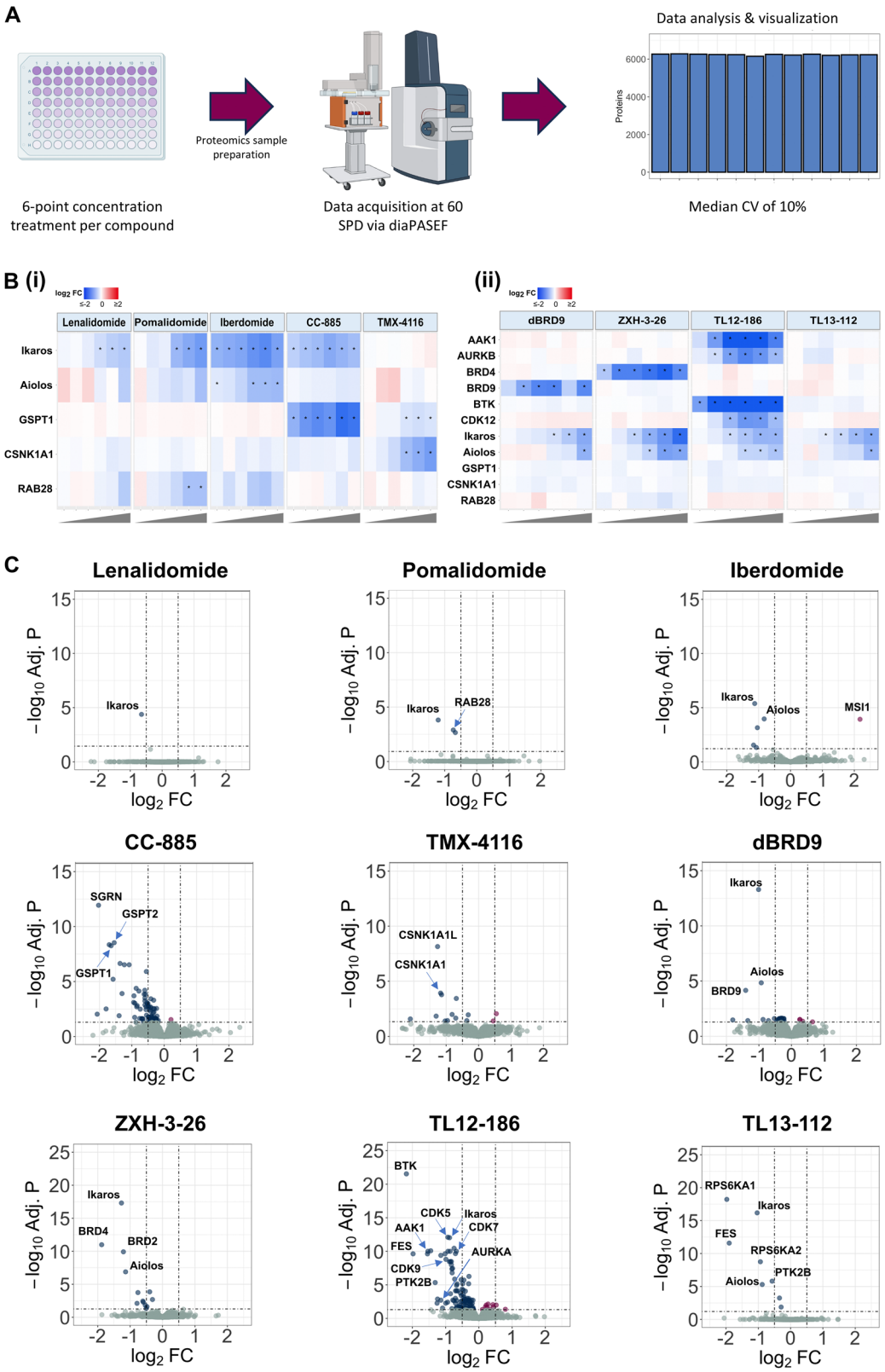

restores the ability of IMiDs like lenalidomide to degrade Ikaros and Aiolos[28]. We have generated a similar transgenic model using a CRISPR knock-in strategy (Supplementary Fig. 4A). Upon a single dose of lenalidomide at 100 mg/kg for 6 h, Ikaros and Aiolos were degraded in the spleen of *Crbn*^{I391V} transgenic mice but not in the wild-type animals, confirming the critical importance of the aa391 for IMiD-induced Ikaros and Aiolos degradation (Supplementary Fig. 4B). Upon 21 days repeat dosing of lenalidomide at 30 and 100 mg/kg, Ikaros and Aiolos were also degraded in the spleen of *Crbn*^{I391V} transgenic mice with the highest dose showing the highest degradation (Supplementary Fig. 4C). In line with previous literature[28], lenalidomide treatment caused a reduction in white blood cells only in the *Crbn*^{I391V} transgenic mice, suggesting a clear link between Ikaros and Aiolos degradation with lymphopenia (Supplementary Fig. 4D).

https://doi.org/10.1038/s41467-026-70663-1

Fig. 1 | IMiD-based PROTAC can degrade IMiD neosubstrates. A Diagram of the proteomic workflow. Created in BioRender. Hamza, G. (2025) https://BioRender.com/sf0sctc. **B** High-throughput proteomics profiling of **lenalidomide**, **pomalidomide**, **iberdomide**, **CC-885** and **TMX-4116** (i) and **dBRD9, ZXH-3-26, TL12-186** and **TL13-112** (ii) in NB-4 cells after 5 h treatment. Statistics calculated using limma's moderated *t*-test (empirical Bayes) with adjusted *p* value using the Benjamini–Hochberg procedure as implemented in the Protti R package (two-sided *p* values). Heatmap representation of five IMiD neosubstrates: Ikaros, Aiolos, GSPT1, CSNK1A1 and RAB28 protein abundance is shown (i) with additional proteins (ii) represented to capture additional protein degradation linked to the primary pharmacology of the PROTACs. $n = 2$ technical replicates per concentration. * indicates statistical significance (moderated *t*-test, 0.05). **C** Volcano plots associated with data presented in (**B**). Each volcano plot depicts the proteomic changes observed at 1 μM with statistics calculated using limma's moderated *t*-test (empirical Bayes) with adjusted *p* value using the Benjamini–Hochberg procedure as implemented in the Protti R package (two-sided *p* values). The blue/magenta colours indicated points of interest based on fold-changes (x-axis) and statistical significance (−log10 of adjusted *p* value, y-axis). Both the *P* value cut-off and fold-change cut off are indicated by dashed lines. A non-comprehensive list of proteins is labelled for demonstration purposes.

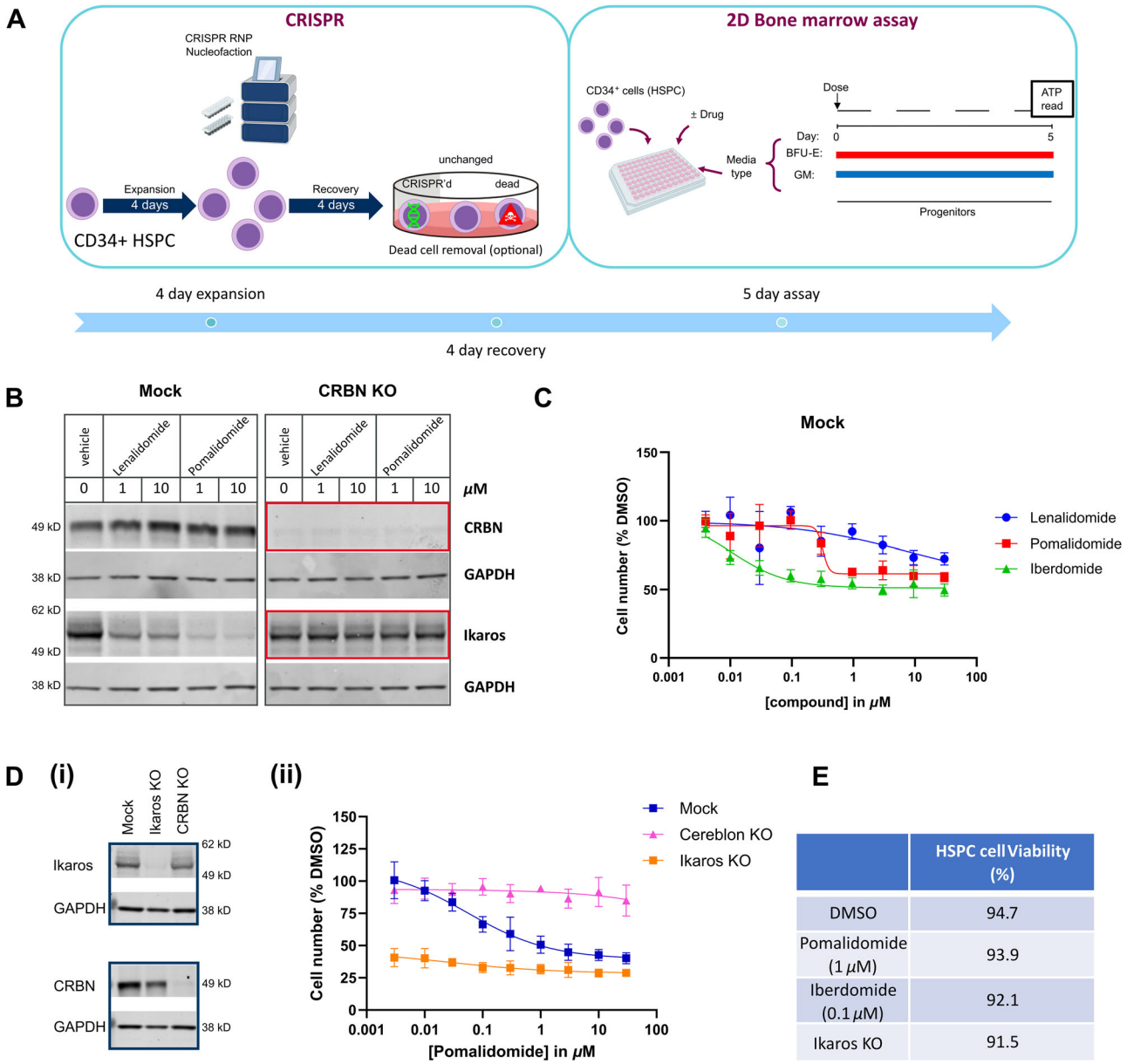

	HSPC cell Viability (%)
DMSO	94.7
Pomalidomide (1 μM)	93.9
Iberdomide (0.1 μM)	92.1
Ikaros KO	91.5

Fig. 2 | IMiDs block the proliferation of hematopoietic stem and progenitor cells through Ikaros degradation. A Schematic representation of the hematopoietic stem and progenitor cells (HSPC) CRISPR targeting and differentiation. Generated by Biorender. **B** SDS-PAGE analysis of Ikaros degradation in HSPC after lenalidomide and pomalidomide treatment for 4 h in CRBN knock-out or mock control conditions. **C** HSPC proliferation assay under lenalidomide (blue), pomalidomide (red) or iberdomide (green) treatment after 5 days of dosing in mock cells. Data are presented as mean values ± SD; $N = 3$ experiments per compound. Source data are provided as a Source Data file. **D** (i) Ikaros and CRBN CRISPR targeting efficiencies are represented in the SDS-PAGE analyses. (ii) HSPC proliferation assay under pomalidomide treatment after 5 days of dosing in mock (blue), CRBN (pink) or Ikaros (orange) knock-out cells. Data are presented as mean values ± SD; $n = 2$ experiments with 6 replicates per treatment condition. Source data are provided as a Source Data file. **E** Cell viability assay measured by flow cytometry at day 5 of the HSPC treated with pomalidomide, iberdomide or the HSPC knock-out for Ikaros. $n = 2$ experiments with 6 replicates per treatment condition.

Identification of an alternative CRBN ligand to reduce IMiD neosubstrate degradation and the associated changes in hematopoietic stem and progenitor cell differentiation

The data above reinforces the link between IMiD-induced hematological toxicity through an MG MoA, with Ikaros as the potential main target involved. It also provides a workflow to screen molecules in vitro that could prove beneficial for identifying CRBN binders for the design of PROTACs with improved safety profiles.

Beyond the safety liabilities introduced by the IMiD moieties, the configurational instability of the chiral centre present on their characteristic glutarimide ring could lead to epimeric mixtures of IMiD-containing PROTACs, thus adding further challenges to their manufacture and clinical development. Finally, the documented chemical instability in different pHs of molecules like thalidomide[30], can introduce further complications in advancing PROTACs to the clinic. Convinced of the effectiveness of CRBN for affecting protein degradation, yet acknowledging the potential disadvantages of introducing IMiD scaffolds to PROTACs, a virtual screening (VS) campaign for the discovery of improved ligands was initiated. This work was in part inspired by a report from the Hartmann group, whereby uracil-containing ligands like uridine were shown by NMR to bind to a bacterial homologue of human CRBN[31]. These scaffolds bind in the same region as thalidomide and with comparable binding affinities.

Intrigued by the potential advantages of uracil-based CRBN ligands (stability and lack of a chiral centre), we curated a focused library of ligands from the AstraZeneca (AZ) collection that bear the common CO-NH-CO pharmacophore present within the glutarimide and uracil rings of the IMiDs and uridine, respectively. Screening this subset, using a previously reported homogeneous time resolved fluorescence (HTRF) assay[32], helped identify the DHU-containing compound **1** as a hit with an IC_{50} of 1.6 μM (Fig. 3A(i) and Supplementary Fig. 5C). This measurable potency—comparable to thalidomide's IC_{50} = 257 nM—and the achiral nature of compound **1**, encouraged us to design a focused library of N1 aryl dihydrouracils. This allowed for the efficient further scoping of the DHU motif as a replacement to the ubiquitous glutarimide present in the IMiDs and the majority of reported CRBN-recruiting PROTACs[33,34].

The screening of this library led to the discovery of compound **2**, which has an IC_{50} of 183 nM in the HTRF assay (Fig. 3A(i) and Supplementary Fig. 5A) and a K_d of 216 nM as determined by isothermal titration calorimetry (ITC) (Supplementary Fig. 5B, C). This indole-substituted DHU is an achiral CRBN ligand with improved affinity, lipophilic ligand efficiency (LLE)[35] and ligand efficiency (LE)[36] compared to thalidomide, making it a worthy contender for incorporation into PROTACs (Table 1). Furthermore, the metabolic stability, as represented by human liver microsomes (HLM) and rat hepatocytes (RH), is improved over thalidomide. More crucially, compound **2** was found to have a superior half-life (>200 h) at pH 7.4 compared to thalidomide (<30 min). This improvement in stability is likely due to: (a) the absence of the hydrolyzable phthalimide group in compound **2** and (b) the stabilising effect the second nitrogen has on the carbonyls of the DHU-ring, making them less susceptible to nucleophilic attack. Exploring potential safety liabilities, compound 2 showed no activity towards cardiac ion channels such as hERG, NaV1.5, Kv4.3 or CaV (Fig. 3A(ii)). When dosed in mice for 24 h at 10, 30 and 100 mg/kg, compound **2** showed dose-dependent plasma Cmax and AUC, with levels higher than those observed with lenalidomide at the same concentrations, demonstrating good properties for oral exposure (Fig. 3B).

Given its favourable physicochemical properties, we tested compound **2** for its ability to degrade IMiD neosubstrates and we found that it does not degrade Ikaros nor Aiolos as measured by immunoblotting in NB-4 cells when tested up to 10 μM (Fig. 3C). To make sure that the lack of degradation was not due to a lack of cell permeability, we performed a competition experiment between compound **2** and the IMiD molecules and an IMiD-based PROTAC (dBRD9) to indirectly assess this. We observed dose-dependent inhibition of Aiolos degradation by compound **2**, irrespective of the initial level of degradation elicited by each compound, confirming that compound **2** binds CRBN intracellularly (Fig. 3D). We further confirmed the inability of **2** in degrading Ikaros and Aiolos in vivo in the spleen of the *Crbn*^{I391V} transgenic mice, even when tested at 100 mg/kg (Fig. 3E). We then profiled compound **2** by deep global proteomics in NB-4 cells, which showed no evidence of reduction of unexpected targets compared to lenalidomide (Fig. 3F and Supplementary Data 2). Furthermore, no effect on the cell numbers of primary HSPCs was observed (Fig. 3G).

To elucidate the role of Ikaros in HSPC differentiation, as well as the potential risk mitigation afforded by compound **2**, we performed a longitudinal phenotypic analysis using high-throughput proteomics following Ikaros depletion, treatment with IMiDs (lenalidomide or iberdomide), or compound **2** during differentiation into erythroid and myeloid lineages (Fig. 4A). In the Ikaros knockout condition, we confirmed successful Ikaros protein depletion at day 0 by CRISPR editing (Fig. 4B). By day 5 of differentiation, we observed widespread proteomic alterations, with significant increase or decrease of numerous proteins in HSPCs differentiating towards both the erythroid and myeloid lineages (Fig. 4B and Supplementary Data 3). Notably, Ikaros knockout led to reduced expression of the transferrin receptor and several hemoglobin subunits (HBD and HBQ1), suggesting impaired generation of red blood cell progenitors (Fig. 4B). We also detected increased abundance of proteins associated with megakaryocyte biogenesis, including integrin αIIb (ITGA2B), integrin βIII (ITGB3), and vinculin (VCL), alongside decreased expression of myeloid markers such as CD48 (SLAMF2) (Fig. 4B). These findings indicate a defect in HSPC differentiation toward erythroid and myeloid fates, with a concomitant shift towards the megakaryocyte lineage.

Consistent with these protein-level observations, Reactome pathway analysis revealed robust enrichment for platelet activation, signalling, and aggregation pathways, components of the hemostasis category, in line with upregulation of megakaryocyte biomarkers (Fig. 4C and Supplementary Data 4). Additionally, we noted upregulation of interferon response pathways, exemplified by increased levels of interferon-induced transmembrane protein 3 (IFITM3) in Ikaros-deficient cells (Fig. 4B, C and Supplementary Data 4). In contrast, pathways linked to transcription, translation, and cell cycle regulation were downregulated (Fig. 4C and Supplementary Data 4).

We next sought to determine the extent to which IMiDs phenocopied the Ikaros knockout condition and, critically, how compound **2** differed from both Ikaros knockout and IMiD treatment. Consistent with their known mechanism of action, lenalidomide and iberdomide both reduced Ikaros protein levels by day 5, while compound 2 had no effect on Ikaros expression (Fig. 5A, B). Assessment of hemoglobin subunits (HBA1, HBQ1, HBB and HBD) and the transferrin receptor revealed that lenalidomide and iberdomide mirrored the reductions observed in Ikaros knockout cells, whereas compound **2** treatment did not alter their expression (Fig. 5A, B). Similarly, biomarkers of megakaryocyte differentiation—including ITGA2B and ITGB3—as well as the interferon response protein IFITM3, were markedly increased in HSPCs treated with IMiDs in both erythroid and myeloid differentiation conditions. In contrast, these changes were not observed following treatment with compound **2** (Fig. 5A). Reactome pathway analysis further supported these findings, showing robust upregulation of platelet activation, platelet signalling, and platelet aggregation pathways (hemostasis) in response to IMiDs, whereas no such enrichment was detected with compound **2** (Fig. 5C and Supplementary Data 4).

Collectively, these findings indicate that IMiDs induce a rewiring of cell differentiation in HSPCs through Ikaros degradation—an effect not observed with compound **2**. To further validate the shift toward the megakaryocyte lineage, we performed single-cell flow cytometry

https://doi.org/10.1038/s41467-026-70663-1

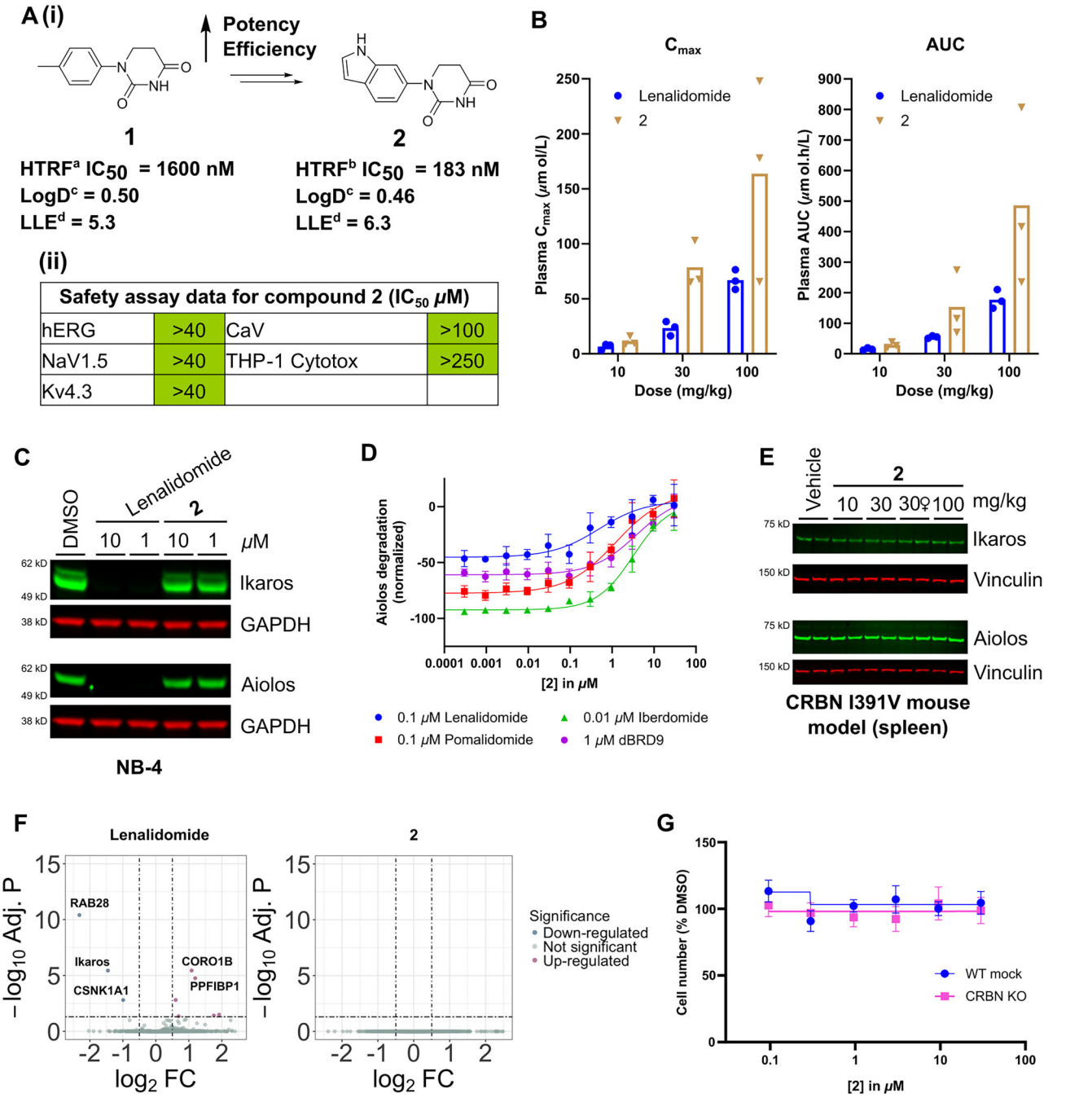

Fig. 3 | Dihydrouracil CRBN binder reduces IMiD neosubstrate degradation and changes in hematopoietic stem and progenitor cell differentiation. A (i) Initial hit (**1**) and its optimisation to the improved CRBN ligand **2**. [a]Activity data based on $n = 2$ with SEM = 0.02 log units. [b] Activity data based on $n = 4$ with SEM = 0.07 log units. [c]LogD measured via shake flask method in octanol and water at pH 7.4. [d]LLE = pIC_{50} − LogD. (ii) Table with compound **2** activity on ion channels associated with cardiovascular toxicities are shown together with a general cytotoxicity assay based on THP-1 viability. **B** Pharmacokinetic profile of lenalidomide (blue) or compound **2** (brown) dosed at 10, 30 and 100 mg/kg for 24 h in mice. $n = 3$ mice per treatment condition. Source data are provided as a Source Data file. **C** SDS-PAGE analysis of Ikaros and Aiolos protein levels in NB-4 cells treated with lenalidomide or compound **2** at 1 μM or 10 μM. $n = 3$ experiments per compound. **D** Aiolos-HiBiT competition assay in MM.1S cells with lenalidomide (blue), pomalidomide (red), iberdomide (green), dBRD9 (purple) and increasing doses of **2**. Dose-response degradation curves normalised to neutral (DMSO, 0%) and max degradation (30 μM pomalidomide, −100%) controls. Data are presented as mean values ± SD; $n = 3$ experiments per compound. Source data are provided as a Source Data file. **E** SDS-PAGE analysis of Ikaros and Aiolos degradation in the spleen of Crbn transgenic (I391V) animals after compound **2** treatment for 6 h at 10, 30 (♀ indicates a female group) or 100 mg/kg. $n = 2$ mice per treatment condition. **F** Deep global proteomics in NB-4 cells after lenalidomide or compound **2** treatment at 1 μM for 24 h. Volcano plots are shown for both molecules. Statistics calculated using limma's moderated *t*-test (empirical Bayes) with adjusted *p* value using the Benjamini–Hochberg procedure (two-sided *p* values). The blue/magenta colours indicated points of interest based on fold-changes (x-axis) and statistical significance (−log10 of adjusted *p* value, y-axis). Both the *P* value cut-off and fold-change cut off are indicated by dashed lines. Protein labels highlight proteins reaching significance. **G** Hematopoietic stem and progenitor cells (HSPC) proliferation assay under compound **2** treatment after 5 days of dosing in mock (blue) or CRBN (pink) knock-out cells. Data are presented as mean values ± SD; $n = 3$ experiments per compound. Source data are provided as a Source Data file.

Table 1 | Property comparison of the IMiD thalidomide versus the dihydrouracil CRBN ligand compound 2

	Thalidomide	Compound 2
HTRF[a] IC_{50} (nM)	257	183
LogD[b]	0.60	0.46
LLE[c]/LE[d]	6.0/0.48	6.3/0.54
MW	258	229
HLM (µL/min/mg)	10.8	<3.0
RH (µL/min/10^6 cells)	2.5	<1.0
Hydrolysis $T_{1/2}$, pH 7.4	<30 min	>200 h
Configurational stability	NO	N/A

[a]Activity data based on $n \geq 4$ with SEM within 0.2 log units. [b]LogD measured via shake flask method in octanol and water at pH 7.4.
[c]LLE = pIC_{50} – LogD. [d]LE = 1.37(pIC50/heavy atoms) with units of kcal mol–1 per heavy atom.

following 5 days of iberdomide treatment or Ikaros knockout, using a panel of antibodies targeting multiple bone-marrow lineages, including megakaryocytes (Supplementary Fig. 6). Consistent with the proteomics data, both Ikaros knockout and iberdomide treatment led to an increase in the proportion of megakaryocytes and a decrease in erythroid while compound **2** showed no effect (Supplementary Fig. 6).

Dihydrouracil-containing PROTACs successfully degrade multiple targets via CRBN engagement

Having demonstrated the benefits of the DHU ligand, it needed to be evaluated within the context of CRBN-recruiting PROTACs to assess its value as a replacement for the popular glutarimide of the IMiDs. In this vein, a co-crystallisation experiment using compound **2** and a bacterial CRBN homologue was attempted in order to reveal the ligand's most amenable position for growth into a PROTAC. From these experiments a 1.39 Å crystal structure was determined, revealing compound **2** to adopt a binding mode for CRBN highly similar to that of thalidomide[31], with no significant conformational changes observed between the two complexes (Fig. 6A). The DHU group mimics thalidomide's glutarimide ring, forming the same hydrogen bonds (shown as black dashes in Fig. 6A) to the backbone carbonyl and NH groups of residues H77 and W79 as seen in the equivalent thalidomide crystal structure (Fig. 6A). Notably, the NH of the indole makes a water-mediated interaction with H56 (Supplementary Fig. 7), which may rationalise the LLE improvement seen when compared to compound **1**. Finally, the proximity of the indole functionality to bulk solvent appeared to allow for growth from any of its relatively exposed N1, C2 and C3 positions. To further evaluate the tolerance of a linking functionality, pendant to these positions, methylacetamides 3, 4 and 5 were synthesised and tested for binding to CRBN (Table 2). The favourable potency of compound **3** helped identify the C3 position of compound **2** as ideal for growth into fully elaborated PROTACs.

The carboxylic acid handle present in compound **3**'s precursor molecule represented an appropriate intermediate for the facile and parallel synthesis of PROTACs via amide coupling conditions. PROTACs containing compound 2 as the CRBN ligand were successfully assessed for a number of targets in the AstraZeneca portfolio, including nuclear receptors[37,38] and epigenetic targets[32]. This evaluation was conducted by employing intermediates bearing ligands to the respective POIs conjugated to amine handles via linkers of varying lengths. A subset of the PROTACs explored, designed to target Bromodomain-containing protein 4 (BRD4), by exploiting the reported JQ1 ligand[39], were synthesised and evaluated for degradation of the target—by Nanoluciferase detection—in a previously reported endogenously HiBiT-BRD4 tagged HEK293 cell line (Fig. 6B)[32,40]. In this instance, the linker length of the explored PROTACs was modulated by varying polyethylene glycol (PEG) units (Fig. 6B). Reassuringly, all the synthesized PROTACs (compounds **6**–**12**, Fig. 6B) maintained the potency of binding to CRBN, thus confirming the C3 position of the indole as an appropriate derivatisation point for PROTAC synthesis. Subsequent evaluation of the PROTACs in the HiBiT-BRD4 cell line revealed that five out of the seven PROTACs are submicromolar degraders with >90% D_{max} values. Intriguingly, compound **6**, which contains the shorter linker, is the most potent PROTAC from this set with a DC_{50} = 172 nM and a D_{max} = 95%, although less potent than the optimised ZXH-3-26 by an order of magnitude (Fig. 6C). To explore the MoA, two negative controls were made to evaluate BRD4 degradation when the binding to CRBN and BRD4 is independently occluded in compound **13** and **14** respectively. As expected, both negative controls showed no activity in the degradation assay, further confirming that compound 6 degrades BRD4 by both direct binding to the selected target and via CRBN. As described earlier, compound 2 alone, showed no neosubstrate degradation in the suite of selected experiments. Importantly, in stark contrast to ZXH-3-26 (Fig. 6C(i)), the DHU-containing compound **6**, and its negative controls (compound 13 and 14), showed no evidence of SALL4 nor Aiolos degradation, supporting the orthogonality of the DHU-containing ligands to the popular IMiDs (Fig. 6C(ii–iv)). When compound **6** was assessed in our high-throughput proteomics assay, we demonstrated its increased selectivity against Ikaros and Aiolos compared to ZXH-3-26 and its overall selectivity with only a few proteins showing a reduction including BRD2, BRD3 and MYC (Fig. 6D and Supplementary Data 5). The reduction of MYC is consistent with the role that BRD4 plays in its transcriptional regulation and, importantly, showcases the advantages of unbiased proteomic analysis achieved in our high-throughput assay[39,41,42].

Discussion

From a drug scandal to established therapies, IMiDs have profoundly influenced the pharmaceutical industry. Initially launched to treat morning sickness, to decades later being the standard of care in MM, IMiDs are now being repurposed within the burgeoning PROTAC[13] and molecular glue[43] modalities. Nevertheless, there is a critical need to assess the risk of IMiD-containing PROTACs in degrading the IMiD neosubstrates—in particular SALL4, Ikaros and Aiolos—and to thoroughly assess the associated toxicities introduced as a consequence of this degradation.

In this manuscript, we show that many IMiD-based PROTACs degrade Ikaros and Aiolos, transcription factors associated with bone-marrow and hematological toxicities. Some IMiD-based PROTACs like ZXH-3-26 were found to be more potent at degrading Aiolos than lenalidomide. There is little doubt now that Ikaros and Aiolos play key roles in hematopoiesis. However, there is still a lack of mechanistic understanding of how IMiDs affect the bone-marrow progenitors. Our high-throughput proteomics approach has shed insights into the effect of lenalidomide and iberdomide on the rewiring of the progenitor's differentiation. It suggests the two IMiDs induce the reprogramming of the cells and most likely cause a defect in the proper differentiation of the bone-marrow progenitors into different blood lineages, as discussed previously[29,44]. It is particularly striking to see an upregulation of megakaryocytic biomarkers together with proteins involved in the interferon response, like IFITM3. IFITM3 has previously been associated with platelet hyperreactivity and thrombosis complications[45]. Interestingly, lenalidomide and pomalidomide have been associated with cardiovascular complications involving thrombosis[26,46,47]. It is therefore attractive to speculate on the effect of a potential bone-marrow progenitor reprogramming towards hyperactivated platelet precursors that could be responsible for cardiovascular complications.

One strategy to mitigate the safety risks associated with the use of IMiDs in PROTACs is to reduce, or ideally eliminate, the degradation of IMiD neosubstrates such as Ikaros. Approaches to address this have included optimising the linker attachment point on the IMiD scaffold,

https://doi.org/10.1038/s41467-026-70663-1

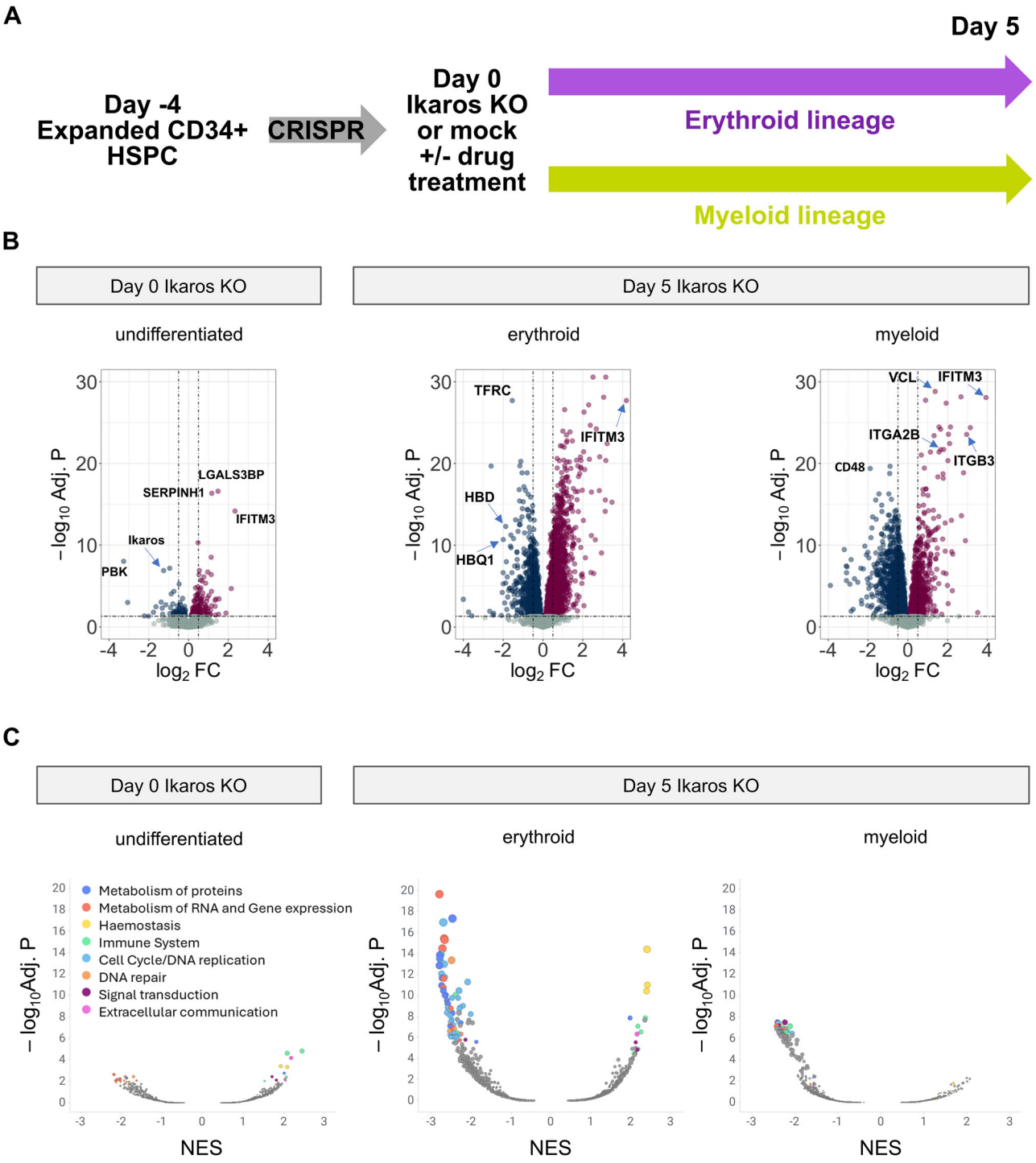

Fig. 4 | Ikaros knock-out affects hematopoietic stem and progenitor cell differentiation. A High-throughput proteomics performed in hematopoietic stem and progenitor cells differentiation assay under lenalidomide, pomalidomide or compound **2** treatment after 5 days of dosing at 1 and 10 μM. One group of cells was knocked out for Ikaros 4 days before the cell differentiation started. Proteomics samples were collected at day −4, day 0 and day 5 after the HSPC differentiation into either the erythroid or myeloid lineages. $n = 4$ replicates per treatment condition. **B** Volcano plots depicting the proteomic changes observed upon Ikaros knock-out. Statistics calculated using limma's moderated *t*-test (empirical Bayes) with adjusted *p* value using the Benjamini–Hochberg procedure (two-sided *p* values). The blue/magenta colours indicate points of interest based on fold-changes (x-axis) and statistical significance (−log10 of adjusted *p* value, y-axis). Both the *P* value cut-off and fold-change cut-off are indicated by dashed lines. A non-comprehensive list of proteins is labelled for demonstration purposes. **C** Corresponding Reactome pathway analysis for plots shown in (**B**). Reactome pathway enrichment was performed using gene set enrichment analysis (fgsea, V1.20.0) on a pre-ranked gene list from (**B**). GSEA was run with min/max gene set sizes of 5/500, respectively and default weighting ($0 \geq p \leq 1$). Normalised enrichment scores (NES) and adjusted *p* value are reported.

https://doi.org/10.1038/s41467-026-70663-1

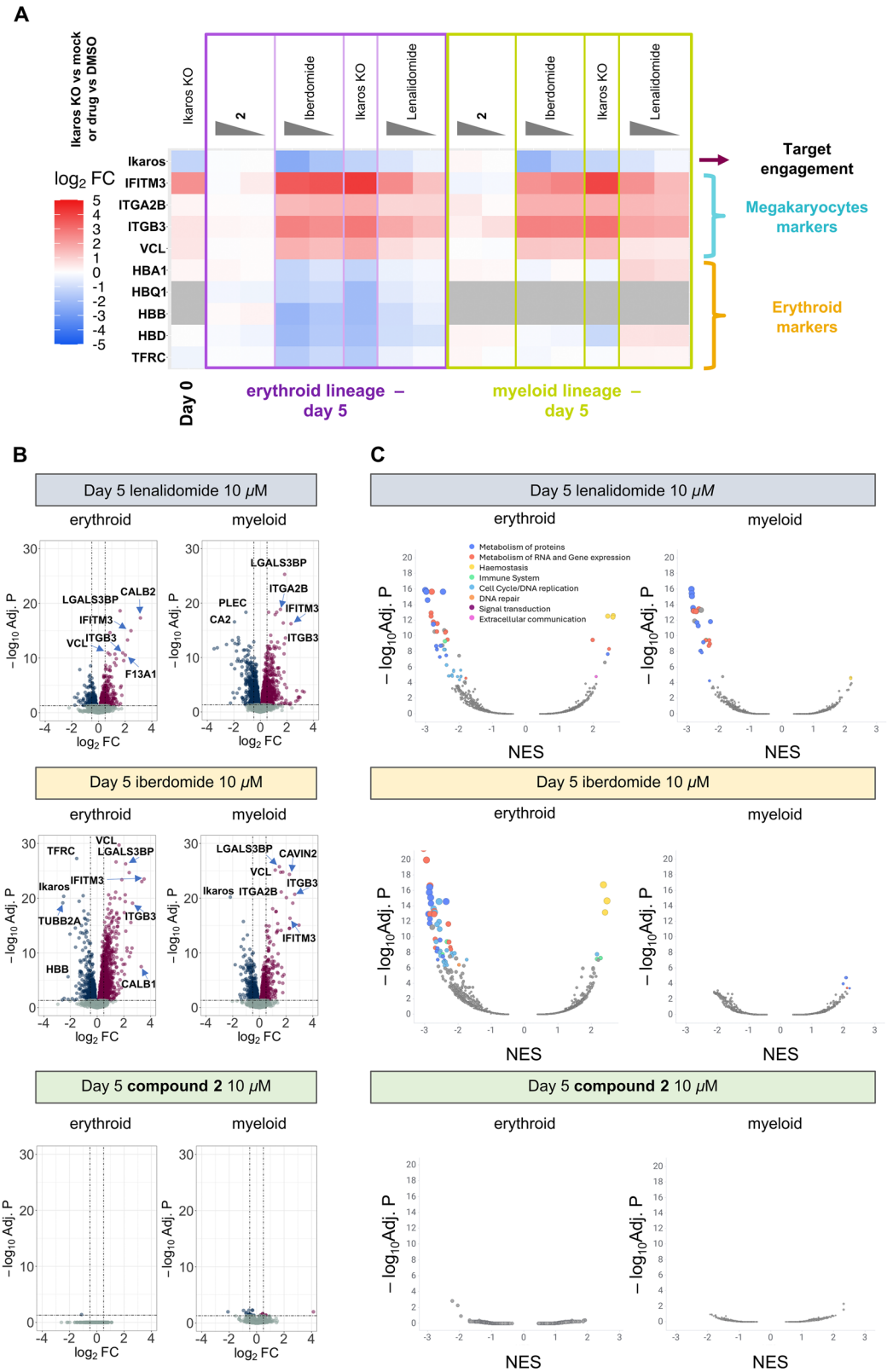

employing benzylamide glutarimide derivatives, developing bump-and-hole thalidomide analogues, and utilising peptidic cyclimide ligands for cereblon engagement[48–51]. However, it remains uncertain whether these strategies can fully prevent the degradation of other, perhaps as-yet-unidentified, CRBN neosubstrates during molecule optimisation. Thus, the use of alternative CRBN ligands represents a preferable route, particularly as the PROTAC modality expands beyond oncology indications.

In this work, we identified alternative CRBN binders featuring a DHU core rather than a glutarimide motif. Notably, a representative CRBN binder—compound **2**—did not induce degradation of the established IMiD neosubstrates Ikaros and Aiolos, nor did it reduce levels of other proteins, as determined by proteomic analysis in the NB-4 leukaemia cell line. As observed with glutarimide-based ligands, where neosubstrate selectivity is influenced by appended functional groups rather than the glutarimide ring itself, it is important to

Fig. 5 | lenalidomide and iberdomide phenocopy Ikaros knock-out changes in hematopoietic stem and progenitor cell differentiation, in contrast to the dihydrouracil CRBN binder. A Heatmap of protein levels focused on Ikaros to demonstrate target engagement, some hemoglobin subunits (HBA1, HBQ1, HBB and HBD) and the transferrin receptor (TFRC) as markers of erythroid differentiation. Some integrin subunits (ITGA2B and ITGB3) are represented as markers of megakaryocyte differentiation together with IFITM3 as an interferon element response upon indicated treatment. **B** Volcano plots showing proteomic changes 5 days post differentiation into either erythroid or myeloid lineages. Treatment conditions are stated above each volcano. Each condition was compared to its equivalent DMSO control. Statistics calculated using limma's moderated *t*-test (empirical Bayes) with adjusted *p* value using the Benjamini–Hochberg procedure as implemented in the Protti R package (two-sided *p* values). The blue/magenta colours indicate points of interest based on fold-changes (x-axis) and statistical significance (−log10 of adjusted *p* value, y-axis). Both the *P* value cut-off and fold-change cut-off are indicated by dashed lines. A non-comprehensive list of proteins is labelled for demonstration purposes. **C** Corresponding Reactome pathway analysis for plots shown in (**B**).

recognise that the DHU scaffold alone does not inherently confer selectivity with regard to molecular glue polypharmacology[52]. Indeed, previous studies have shown that DHU-based CRBN ligands, bearing alternative N1 position substituents, can themselves function as molecular glue degraders for various neosubstrates[53].

Although compound **6**, as described in this manuscript, lacked the requisite properties for advancement into in vivo studies, our results—together with the successful design of DHU-containing active degraders for other targets within the AstraZeneca portfolio—underscore the potential of this CRBN ligand[37,38]. We are confident that this scaffold can facilitate the development of chemically and configurationally stable, potent, and selective PROTACs, ultimately contributing to improved safety profiles for future therapeutics.

Methods

Ethics statement

All animal work has been approved by the Animal Welfare Ethical Review Body at the Babraham Institute under the project license PPL PP7736793. Housing conditions: up to five animals per cage, in individually ventilated cages, aspen bedding, ad libitum complete diet, water at 19 ± 2 °C and humidity at 55 ± 10% with a 7 am/7 pm dark/light cycle.

Human bone marrow-derived donor cells used in this research were obtained under approved informed consent at the time of initial collection, with donors providing explicit permission for the use of their samples in research, including downstream applications. This is consistent with AstraZeneca (AZ) requirements that informed consent must be in place for the proposed use of human biological samples (HBS). All samples are classified as human biological samples (HBS) and are handled in accordance with applicable ethical guidelines, AZ policy and standards for HBS, and relevant regulatory requirements governing the use, storage, and tracking of human donor material. Donor information is coded and nonidentifiable, and no attempts are made to reidentify donors in accordance with AZ's principles of sample stewardship and data protection. The ethical approval and consent for the initial collection and storage of these samples were confirmed through AZ's due diligence processes with the original sample provider, as required under AZ governance frameworks for HBS sourcing. Where applicable, future-use consent covers the research conducted in this project, and internal governance review has confirmed that the planned work falls within the scope of permitted use under the original consent documentation. All research using these samples is conducted in accordance with ethical principles aimed at safeguarding donor rights and ensuring responsible scientific practice. The project complies with AZ processes that govern the ethical re-use of HBS, which include ensuring that samples are used only within the scope defined by consent and any relevant Research Ethics Committee or Institutional Review Board determinations.

Cell lines, primary HSPCs, cell culturing and in vitro differentiation

Bone marrow-derived CD34+ human hematopoietic stem/progenitor cells (HSPCs) (2M-101, Lonza) were cultured in expansion medium (StemSpanTM SFEMII, 09655, STEMCELL Technologies) supplemented with Stem Span™ CD34+ Expansion Supplement (02691, STEMCELL Technologies). For in vitro differentiation to the erythroid and myeloid lineages the HSPCs were resuspended in either BFUE-1 (SEC-BFU1-40H), or GM-CFC (SEC-GM1-40H) CellExpandTM Suspension Expansion Culture (SEC, Preferred Cell Systems) for 5 days.

HiBiT-IKZF3 MM.1S cells (obtained from Promega, CS3023229) were grown in RPMI-1640 (Gibco), supplemented with 10% FBS and GlutaMAX (Gibco). HiBiT-SALL4 SK-N-DZ cells (obtained from Promega, CS3023238) were grown in DMEM (high glucose) (Gibco), supplemented with 10% FBS, GlutaMAX (Gibco), sodium pyruvate (1 mM) (Gibco) and 1% non-essential amino acids (NEAA) (Sigma). HiBiT-BRD4 cells were generated via CRISPR-CAS9 knock-in of the HiBiT tag at the N-terminus of endogenous BRD4 in HEK293 cells (DSMZ, ACC-305. A single clone was expanded, and a bank of cryopreserved cells was generated. NB-4 cells (obtained from DSMZ, ACC-207) were grown in RPMI-1640 (Gibco), supplemented with 10% FBS and Glutamax (Gibco). All immortalised cell lines used in this study were tested by STR (short tandem repeat) Fingerprint.

Competition experiments

HiBiT-IKZF3 MM.1S cells were started from cryovials into media and dispensed onto a 384-well plate at 20k cells/well using a multidrop combi. IMiDs and dBRD9 were added at concentrations needed to elicit >50% degradation of Aiolos (iberdomide 0.01 μM, lenalidomide and pomalidomide 0.1 μM, dBRD9 1 μM). Alongside those compounds, **2** was added in a 12-point, half-log dose-response with a top concentration of 30 μM. Wells were backfilled with DMSO. DMSO and pomalidomide (30 μM) were used as spot controls across the plates to define the scale range. Plates were subsequently spun for 1 min at 300×*g* and incubated for 6 h at 37 °C, 5% CO_2 in a humidified incubator. HiBiT Lytic Detection Reagents (Promega) was prepared according to the manufacturer's instructions, and 5 μL/well of the lytic detection mix was added to each plate using a multidrop combi. Plates were spun for 1 min at 300×*g*, placed on an orbital shaker at 300 rotation per minute (rpm) for 30 min before reading luminescence on an Envision-1 plate reader according to the manufacturer's instructions. Data analysis was carried out as described in the supplemental information.

CRISPR-Cas9 editing in human primary CD34+ human hematopoietic stem and progenitor cells

CD34+ human hematopoietic stem and progenitor cells (HSPCs) were cultured for 4 days in expansion medium prior to CRISPR-Cas9 gene editing based on methods described previously[54–56]. RNP synthesis was performed by incubating a pool of guide RNAs (120 pmol) targeting either CRBN or Ikaros (sequences in Table 3) with 10^5 pmol Alt-R® S.p. Cas9 Nuclease V3 protein (IDT) at room temperature for 10–20 min. HSPCs were resuspended in P3 transfection buffer (Lonza) containing 5 μM carrier DNA at 3×10^5 cells per 20 μL sample before being transfected with 5 μL RNP or with Cas9 only (mock) using programme DZ-100 on the 4D-Nucleofactor system (Lonza). Following transfection, the cells were resuspended in expansion medium and cultured for 4 days. Knockout of CRBN, or Ikaros protein, was determined as stated in the Western Blot section.

Human hematopoietic stem and progenitor cells (HSPC) erythroid and myeloid differentiation/proliferation assay

Human hematopoietic stem and progenitor cells (Mock, CRBN KO, Ikaros KO) were resuspended in BFUE-1 SEC (SEC-BFU1-40H)

https://doi.org/10.1038/s41467-026-70663-1

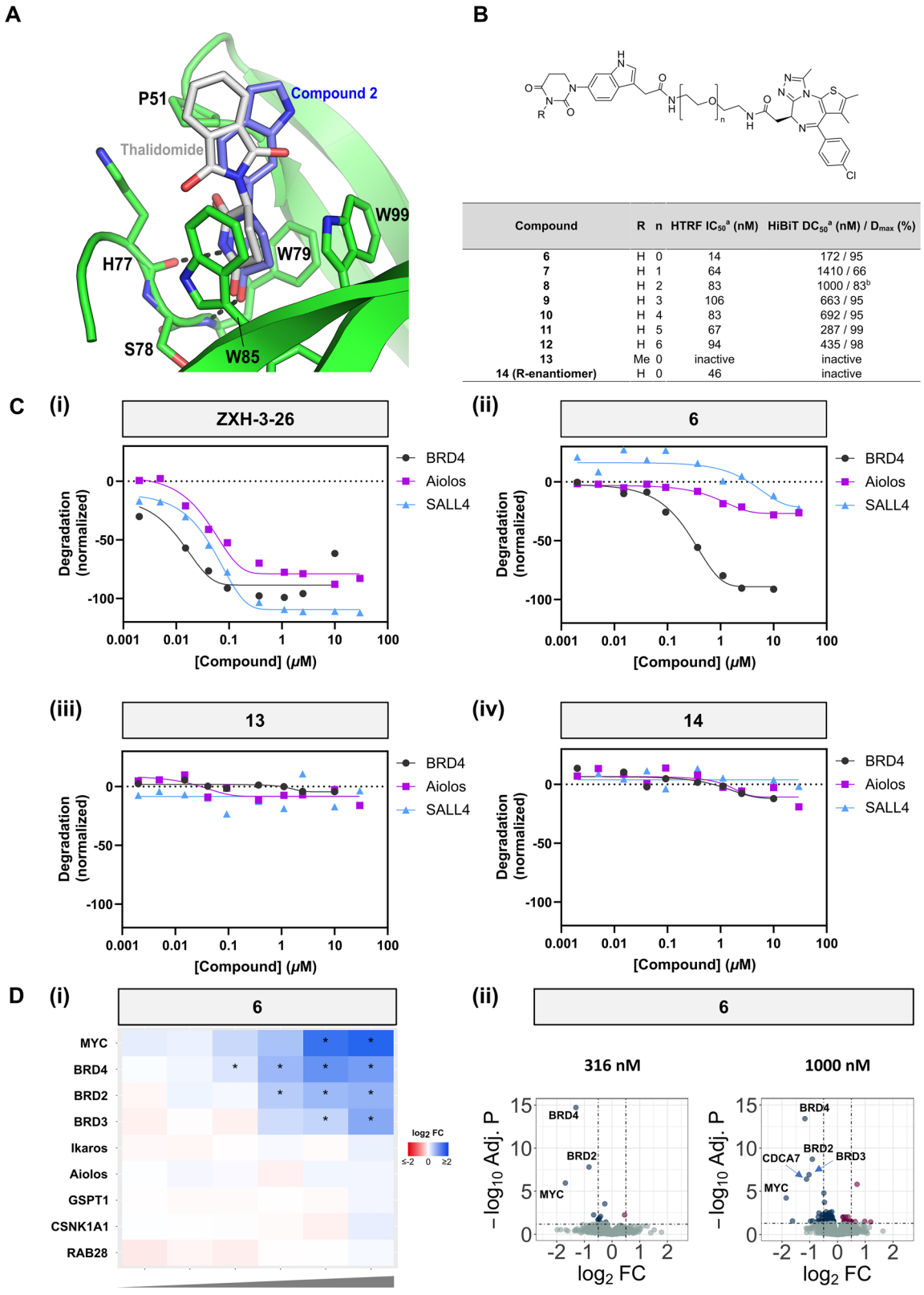

Compound	R	n	HTRF IC_{50}[a] (nM)	HiBiT DC_{50}[a] (nM) / D_{max} (%)
6	H	0	14	172 / 95
7	H	1	64	1410 / 66
8	H	2	83	1000 / 83[b]
9	H	3	106	663 / 95
10	H	4	83	692 / 95
11	H	5	67	287 / 99
12	H	6	94	435 / 98
13	Me	0	inactive	inactive
14 (R-enantiomer)	H	0	46	inactive

CellExplandTM Suspension Expansion Culture (SEC, Preferred Cell Systems) 4 days post-transfection (1×10^4/mL) in the presence or absence of compounds and plated out at 500 cells per well of a 96-well plate. After 5 days of incubation, the number of viable cells per well was determined using CellTiter-Glo® 2.0 (G9242, Promega) with the luminescence readout being performed on an Envision plate reader (Perkin Elmer). Data was normalised to the vehicle control (DMSO). Curves were generated using non-linear regression (curve fit) analysis (Graphpad Prism 9). To assess the viability of the cells, cells were stained with the primary amine-reactive Live/Dead Fixable yellow dead cell stain kit (Thermo Fisher L34959). Briefly, cells were washed once (300×*g*, 5 min, 4 °C), resuspended in PBS-0.5% BSA and placed on ice. Samples were stained with viability dye at 4 °C for 30 min in the dark. Samples were washed twice and resuspended in PBS-0.5% BSA. Cells

Fig. 6 | PROTACs bearing the dihydrouracil-containing CRBN binder successfully degrade BRD4 whilst sparing the IMiD-associated neosubstrates Aiolos and SALL4. A Crystal structure of CRBN bound by compound **2** (green and blue carbons, respectively, PDB entry 9GJQ) overlaid with the crystal structure of CRBN bound by thalidomide (white carbons, PDB entry 4V32, protein not shown). Hydrogen bonds from the DHU group of compound **2** to CRBN are shown as black dashes. **B** CRBN binding and BRD4 degradation evaluation of DHU-containing BRD4-targeting PROTACs. [a]Activity data based on $n = 3$ with SEM within 0.2 log units, unless otherwise stated; [b]$n = 2$. **C** Dose-response curves of the BRD4 (grey), Aiolos (purple) and SALL4 (blue) HiBiT assays are represented in the graphs and normalised to neutral (DMSO, 0%) and max degradation (30 μM pomalidomide, −100%) controls for: (i) **ZXH-3-26**, (ii) **6** (BRD4 and CRBN active), (iii) **13** (CRBN inactive) and (iv) **14** (BRD4 inactive). $n = 3$ experiments per compound. **D** (i) Heatmap representation of protein abundance of five IMiD neosubstrates: Ikaros, Aiolos, GSPT1, CSNK1A1 and RAB28, plus the primary target BRD4, and its close homologues, BRD2 and BRD3 and downstream target MYC. * indicates statistical significance (moderated *t*-test, 0.05). $n = 2$ technical replicates per concentration. (ii) Each volcano plot depicts the proteomic changes observed for compound **6** at 316 and 1000 nM. Statistics calculated using limma's moderated *t*-test (empirical Bayes) with adjusted *p* value using the Benjamini–Hochberg procedure as implemented in the Protti R package (two-sided *p* values). The blue/magenta colours indicated points of interest based on fold-changes (x-axis) and statistical significance (−log10 of adjusted *p* value, y-axis). Both the *P* value cut-off and fold-change cut-off are indicated by dashed lines. A non-comprehensive list of proteins is labelled for demonstration purposes.

Table 2 | Structure–activity relationship exploration of dihydrouracil-containing CRBN binders for elaboration into PROTACs

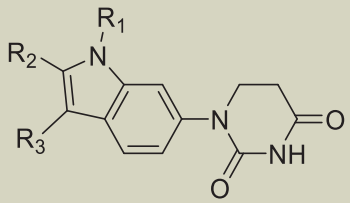

Compound	R_1	R_2	R_3	HTRF[a] IC_{50} (nM)	LogD[b]	LLE[c]
2	H	H	H	183	0.46	6.3
3	H	H	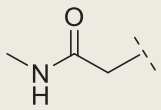	286	−0.80	7.3
4	H	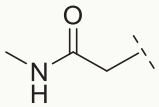	H	939	−0.45	6.5
5	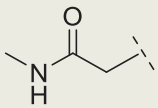	H	H	2170	−0.48	6.1

[a]Activity data based on $n \geq 2$ with SEM within 0.2 log units. [b]LogD measured via shake flask method in octanol and water at pH 7.4.
[c]LLE = pIC_{50} − LogD.

were fixed by the addition of an equal volume of 4% PFA (Thermo Fisher) for 15 min at RT. Cells were washed twice and resuspended in PBS-1% BSA before acquisition on the BD LSR Fortessa (BD Biosciences). Data were analysed using FloJo 10 (FlowJo LLC).

HSPCs were cultured in expansion medium (StemSpanTM SFEMII, 09655, STEMCELL Technologies) supplemented with Stem Span™ CD34+ Expansion Supplement (02691, STEMCELL Technologies). For in vitro differentiation to the erythroid and myeloid lineages the HSPCs were resuspended in either BFUE-1 (SEC-BFU1-40H), or GM-CFC (SEC-GM1-40H) CellExpandTM Suspension Expansion Culture (SEC, Preferred Cell Systems) for 5 days. Treatment with either DMSO, lenalidomide, iberdomide or **2** using 1 and 10 μM for 5 days was performed during the differentiation phase. For each condition, HSPCs ± Ikaros KO were plated in 96-well plates to obtain min. 15k cells per well at harvesting time. High-throughput proteomics was carried out as described below.

Independent samples were generated for flow cytometry analysis of differentiated cells by plating 5000 cells (for BFUE) or 10,000 cells (for GM) per well of a 24-well plate. Ikaros KO cells, generated as above, and Mock cells treated with either DMSO, iberdomide or compound **2** using 10 μM were cultured for 5 days in differentiation media.

Staining procedure. Cells were washed once (300×*g*, 5 min, 4 °C), resuspended in cold PBS-0.5% BSA and maintained cold. Cellular expression of surface antigens was determined using flow cytometry. Reference controls for spectral unmixing were prepared alongside the samples using UltraComp eBeads™ Plus Compensation Beads (Thermo Fisher 01-3333-42) for the CD markers and cells for the viability and EdU reference controls. Group-specific unstained reference controls were prepared to allow spectral unmixing incorporating condition-specific autofluorescence. Independent FMO controls were prepared alongside the samples and reference controls for BFUE media- and GM media-cultured cells to aid in gating accuracy. Antibodies and Viability dye were dispensed using the Dragonfly® Discovery (sptlabtech) liquid dispenser into a 96-well plate, into which the staining was carried out. The cells were incubated for 30 min at 4 °C in the dark with the antibody cocktail. Samples were washed twice and resuspended in PBS-0.5% BSA. Samples were subsequently washed with wash buffer containing DPBS (Gibco) with 0.5% BSA (Sigma), 5 mM EDTA (Thermo Fisher) and 25 mM HEPES (Sigma) and fixed with 2%. Cells were fixed with PFA (Thermo Fisher) for 20 min at RT. Samples were then washed and resuspended in acquisition buffer containing DPBS (Gibco) with 0.5% BSA (Sigma), 5 mM EDTA (Thermo Fisher) and 25 mM HEPEs

(Sigma) before acquisition. All plate washes were performed using the Curiox HT2000™ (Curiox BioSystems; settings: nine washes at 5 uL/s performed after staining and fixation). Samples were analysed using the Cytek Aurora™ 5 L (Cytek Biosciences) spectral flow cytometer, spectral unmixing was performed on the SpectroFlo software (Cytek Biosciences), and analysis was carried out using OMIQ™ (Dotmatics). The list of antibodies used to identify the different cell populations is available in Table 4, and the gating strategy is described in Supplementary Fig. 9 (See Supplementary Note).

Proteomics

High-throughput proteomics. NB-4 cells were cultured in 96-well plates to obtain 200k cells per well and subsequently treated with PROTAC compounds for 5 h using a dose-response concentration format (0.003, 0.01, 0.03, 0.1, 0.316, 1 μM). Human hematopoietic stem and progenitor cells (HSPCs) samples were detailed above.

Cells were washed twice with ice-cold PBS and were snap frozen at −80 °C. Cell pellets were lysed, and proteins were reduced and alkylated using a one-pot buffer (PreOmics® iST). Proteins were proteolysed into peptides using trypsin: LysC through overnight digestion, and subsequently, peptides were cleaned up on a styrene-divinylbenzene-based sorbent (PreOmics®). Peptides were loaded onto EvoTips (EvoSep Biosystems®) and were analyzed using an EvoSep One® liquid chromatography (LC) system connected to a timsTOF Flex® mass spectrometer (MS) (Bruker Daltonik) through an 8 cm × 150 μm, 1,5 μm C18 based column (EvoSep Biosystems®). The LC was operated using the 60 samples per day (SPD) method (NB-4) or 30 SPD (HSPCs), while mass spectra was acquired using data-independent acquisition parallel accumulation-serial fragmentation (diaPASEF) using a window schema constructed using py_diAID[57]. Data processing was conducted using DIA-NN[58], while differential expression, statistical analysis and visualisation was conducted using a custom-based R script[59].

Table 3 | RNA/DNA sequences of components from the CRISPR/Cas9 experiments

Name	Sequence
CRBN single guide RNAs (Synthego KO kit v2)	CGCACCAUACUGACUUCUUG GUGAUGAUGAUCCUGAUUCC AUAGUACCUAGGUGCUGAUA
Ikaros guides single guide RNAs (Synthego KO kit v2)	UGUCGUAGGGCGUGUCGGAC CAACAACGCCAUCAACUACC ACCACCUCGGAACCGCCCGG
Carrier DNA	CCAGCAGAACACCCCCATCGGCGAC GGCCCCGTGCTGCTGCCCGACAACCA CTACCTGAGCACCCAGTCCGCCCTGAGC AAAGACCCCAACGAGA

Deep global proteomics

Sample preparation and digestion. NB-4 cell extracts were prepared using the iST 96x sample preparation kit according to the manufacturer's instructions (PreOmics®). In short, cell pellets were lysed by resuspension in a lysis buffer solution and heated to 95 °C for 10 min shaking (1000 rpm), followed by pulsed sonication (10 × 1 s pulses, Qsonica). Aliquots containing 50 μg of protein were transferred into cartridges, and the digestion solution was added, and proteins were digested for 4 h at 37 °C. Digestion was stopped by adding 'stop' solution and peptides were purified by centrifugation for 2 min at 2000×*g*, followed by two washes and elution into a collection plate using the provided solutions. Peptides were dried in a vacuum centrifuge and resuspended in 0.1% formic acid, 2% acetonitrile (ACN) for MS analysis.

LC-MS/MS analysis. Nanoflow LC-MS/MS was performed by coupling an UltiMate ™ 3000 RSLCnano system (Thermo Scientific) to an Orbitrap Eclipse ™ mass spectrometer (Thermo Scientific). Two μg of peptides were trapped on an Acclaim Pepmax column (2 cm × 75 μm, 3 μm, 100 Å) in water with 0.1% formic acid (FA) and separated on a C18 Aurora column (25 cm × 7.5 μm, 1.7 μm, IonOpticks) at 50 °C. Gradient elution was performed from 5% ACN to 27% ACN in 0.1% FA over 100 min at a 400 nL/min flow rate. The mass spectrometer was operated in data-independent acquisition (DIA) mode with full scan MS spectra acquired at 120,000 resolution and AGC target at 100%. MS2 spectra were collected at 15,000 resolution, AGC target at 100% and normalised collision energy set at 28%. Seventy-five variable windows covering a mass range of 400–1000 m/Z and with an overlap of 1 m/z were used. Default settings were used for FAIMS and three CV values (−45, −55, −75) were set.

Data processing and bioinformatics. Raw files were searched with Pulsar embedded in Spectronaut (version 17.3) against a UniProt human database (February 2021) using the directDIA workflow and default BGS factory settings. Global imputation of missing intensities and cross-run normalisation were performed using Spectronaut processing. Statistical analysis was carried out using in-house scripts with linear models (limma) and false discovery rate (FDR)-adjusted *p* values were calculated using the Benjamini–Hochberg procedure, *p* values less than 0.05 were considered statistically significant.

Animal studies

***Crbn*^{I391V} knock-in transgenic mouse line generation.** *Crbn*^{I391V} KI mice were generated using the CRISPR-Cas9 technology. A RNP, ribonucleoprotein, complex was formed using a single guide, sgRNA, in complex with SpCas9, (IDT: Alt-R™ S.p. Cas9 Nuclease). The Crbn I391V point mutation was introduced by mixing (1:1 ratio) a single-stranded DNA, ssDNA, template and two annealed oligos. Both harbouring the I391V point mutation as well as homology sequences

Table 4 | List of antibody/dye used for the flow cytometry gating strategy

#	Antibody/dye (clone)	Supplier	Catalogue #	Dilution used per 25-μL cell suspension
1	**CD34:APC-Cy7 (561)**	BioLegend	343614	3.75 μL of 1X
2	**CD38:PE (HIT2)**	BioLegend	303506	2.5 μL of 1:4
3	**CD36:BV421 (5-271)**	BioLegend	336230	2.5 μL of 1:4
4	**CD235a:BV786 (GA-R2 (HIR2))**	BD	740984	2.5 μL of 1:5
5	**CD41:APC (HIP8)**	BioLegend	303710	2.5 μL of 1:4
6	**CD71:BUV395 (M-A712)**	BD	743308/new 568523	2.5 μL of 1X
7	**CD16:BV480 (3G8)**	BD	566108	2.5 μL of 1:5
8	**CD13:BUV737 (WM15)**	BD	741828	2.5 μL of 1:10
9	**CD42b:BV711 (HIP1)**	BD	740779	2.5 μL of 1:4
10	**LIVE/DEAD Aqua**	Thermo	L34966	1.5 μL of 1:10

directed towards the *Crbn* gene. The oligos are complementary except for the last 30 bp on each strand, giving rise to a partly double stranded donor template with 30 bp single stranded 3 prime overhangs (see below). Along with the point mutation, a restriction fragment length polymorphism (RFLP) site is generated (HpyCH4II) that could be used for genotyping of the mouse line.

About 100 cryopreserved C57Bl6/N mouse zygotes, purchased from Janvier Labs, SE-ZYG-CNG, were used for the *Crbn*^{I391V} model generation. 50 zygotes /shot were placed in a 1 mm BIORAD GenePulser®Micropulser ™ cuvette containing 10 μL Optimem and 10 μL RNP complex (6 μM Cas9;6 μM sgRNA) + DNA donor mix (15 μM). The BIORAD Gene Pulser Xcell Electroporation system was used to electroporate Zona intact embryos, with the following settings: Square wave protocol, Voltage 30 V, Pulse length 3 ms, Number of pulses 10, pulse interval 100 ms, cuvette length 1 mm. After electroporation, 100 μL KSOM + AA was used to transfer zygotes from the electroporation cuvette to prewarmed KSOM in embryo dishes. The zygotes are left to recover in a water jacket incubator at 37 °C and 5% CO_2 overnight. Zygotes that developed into two-cell stage embryos were implanted into pseudo-pregnant, B6D2F1/CRL, Charles River Laboratories, foster mothers. Born pups were analyzed for harbouring the point mutation, by Sanger sequencing. Founders were bred to C57Bl6/N, CRL, mice to establish germline transmission and line expansion.

Offspring were genotyped using primers Crbn F2; gcatctccaacagaaatggagaa and Crbn R2; gggcagatctgacttgaggaaat, giving rise to a 433 bp long PCR product. The PCR fragment can either be used for sequencing or restriction digestion using HpyCH4II. Alleles carrying the *Crbn* I391V point mutation will be digested and give rise to two bands, 211 bp and 222 bp in length.

Annealed ss ds ss oligos. ----------CTTCATTTTA-TAGGTATGCATGG*AC**A**G*TTGCCCAGTGCAA***A***AT***T***TGTGCAAGCCA-TATTGGATGGAAATTTACAGCCACAAAAAAAGACATGTCACCTCA

CGATTTTTATCCAAAATTGAATATAGAAAGGAAGTAAAA-TATCCATACGTACC*TG**TC***AACGGGTCACGTT***T***TA***A***ACACGTTCGGTA-TAACCTACCTTTAA----------

ssDNA oligo donor. TGTAAATTTGAGGTGTCAGAGAAATCTCACGA-GAAGCCTAGTACAAAGGCTAAAAATAGGTTTTAACTTA-TATCTTTCCTTCATTTTATAGGTATGCATGGA-C***A******G***TTGCCCAGTGCAA***A***AT***T***TGTGCAAGCCA-TATTGGATGGAAATTTACAGCCACAAAAAAAAGA-CATGTCACCTCAAAAATTTTGGGGCTTAACTCGCTCTGCTCTGT-TACCCACAATTCCAGAGACTGAAGATGAAATAAGT

ss ds ss Crbn Oligo donor Forward. CTTATATCTTTCCTTCATTTTA-TAGGTATGCATGGAC***A******G***TTGCCCAGTGCA***A***AAT***T***TGTGCAAGCCA-TATTGGATGGAAATTTACAGCCACAAAAAAAGACATGTCACCTCA

ss ds ss Crbn Oligo donor Reverse. AATTTCCATCCAA-TATGGCTTGCACA***A***AT***T***TTGCACTGGGCAACTGTCCATGCATACCTA-TAAAATGAAGGAAAGATATAAGTTAAAACCTATTTTTAGC

sgRNA ACAGATCTTGCACTGGGCAA. Silent point mutation (T390T AC***C***→AC***A***; to destroy NGG PAM site for SpCas9, L395L AA***G***→AA***A*** and I396I, AT***C***→AT***T*** to introduce silent mutations in sgRNA binding site) in bold Italic I391V point mutation in bold (**A**TT→**G**TT). ss single strand, ds double strand. Grey; sgRNA binding site reverse strand.

Lenalidomide and compound 2 treatment: blood sample and tissue collection

Lenalidomide and compound **2** were dosed in C57BL/6 mouse wild-type or *Crbn*^{I391V} knock-in model at 10, 30 and 100 mg/kg using oral gavage. The formulation contained 0.5% HPMC + 0.1% Tween80 in MQ water. Blood samples were taken via tail prick and collected into hematocrit tubes containing EDTA. Plasma was prepared by centrifugation (1500×*g*, 10 min, 4 °C). After centrifugation, the blood cell phase was collected with a microcapillary (non-EDTA treated). For necropsy and tissue collection, the animals were terminated via administration of isoflurane. The spleens were rinsed with sterile 1x PBS and frozen on dry ice for storage at −80 °C.

Plasma analysis. Plasma was prepared within 30 min of blood sampling by centrifugation (1500×*g*, 10 min, 4 °C). 8 μL of plasma was collected with a micropipette (Non-EDTA treated, Ref no 172292, Vitrex Medical A/S, Denmark), from the hematocrit tube. The micropipette containing plasma was placed in a 0.5 mL U-shaped polypropylene cryotube (Sarstedt Microtube with cap Ref#72.730) and immediately frozen.

Blood count analysis. Peripheral blood samples were collected at Day 21 after cardiac bleed under terminal isoflurane/oxygen anaesthesia and mixed with EDTA anticoagulant. The samples were then analyzed by spectrophotometry, sheath flow direct current detection, and fluorescence flow cytometry for a full hematological blood count using a Sysmex XN-V hematology analyzer (Sysmex Corporation).

Western blots

Animal samples. Spleens from treated animals were lysed in RIPA buffer (Thermo Fisher) supplemented with 1x Halt Protease and Phosphatase inhibitor cocktail (Thermo Fisher) at a ratio of 150 μL buffer per 100 mg of tissue. A plastic pestle was used to disrupt the tissues and they were allowed to lysed on ice for 15 min. Lysates were centrifuged at 20,000×*g* for 10 min at 4 °C to remove insoluble material. About 40 μg of total protein was run on a 4–12% Bis-Tris gel (Thermo Fisher) with the addition of 4 x LDS sample buffer (Thermo Fisher) and 10 x NuPage reducing agent (Thermo Fisher). Samples were resolved at 150 V for 80 min before transfer to nitrocellulose membrane using the iBlot 2.0 gel transfer system (Thermo Fisher). Membranes were stained with Revert Total Protein stain (Li-Cor) prior to blocking with Intercept Blocking Buffer (Li-Cor). Membranes were incubated with antibodies against Ikaros (14859S, CST, 1:1000 dilution), Aiolos (15103S, CST, 1:1000 dilution), and Vinculin (V9131, Sigma, 1:10,000 dilution) overnight at 4 °C. Membranes were washed 3 x TBS-Tween before incubation with secondary antibodies IRDye 800CW anti-rabbit (926-32213, Li-Cor, 1:10,000 dilution) and IRDye 680RD anti-mouse (926-68072, Li-Cor, 1:10,000 dilution). Membranes were washed 3 x TBS-Tween and imaged on the Odyssey CLx and ImageStudio Software v5.2. Scans were exported to Empiria Software v2.2 (Li-Cor) for quantification.

Cell lines. For Ikaros assessment, NB-4 cells were seeded in 12-well plates at a density of 0.5×10^6 cells/ml per well in 1 mL of RPMI-1650 (10% FBS, 1% Glutamax) and incubated overnight at 37 °C, 5% CO_2 in a humidified incubator. Cells were treated with compounds as indicated (vehicle DMSO, final % up to 0.1%) and incubated for a further 24 h prior to harvest. NB-4 cells were directly transferred to a 1.5 mL microcentrifuge tube, centrifuged at 500×*g* for 5 min, and washed with 1 mL PBS. The cell pellets were resuspended in 50 μL of RIPA buffer supplemented with 1 x Halt Protease and Phosphatase inhibitor cocktail and lysed on ice for 15 min. Lysates were centrifuged at 20,000×*g* for 10 min at 4 °C to remove insoluble material. About 10 μL of lysate was loaded per well with 4 x LDS sample buffer and 10 x reducing agent. Samples were resolved as stated above and the immunoblot carried as described, with the exception that GAPDH (60004, Proteintech, 1:5000 dilution) was used instead of Vinculin and primary antibodies Ikaros (14859S, CST, 1:1000 dilution) were utilised for NB-4. Knockout of CRBN, or Ikaros, in HSPC was assessed via immunoblotting. Samples were resolved as stated above and the immunoblot carried as described, with the exception that GAPDH (ab181602,

Abcam, 1:10,000 dilution) was used for normalisation and primary antibodies against CRBN (71810S, CST, 1:1000 dilution) were utilised for HSPC.

Uncropped and unprocessed scans can be found in the Supplementary Information.

Nanoluciferase assay. Compound assay-ready-plates were prepared using acoustic dispensing (Echo), generating 12-point, half-log dose-responses with a top concentration of 30 μM. Wells were backfilled with DMSO to 0.3% DMSO. DMSO and Pomalidomide (30 μM) were used as neutral (0) and 100% degradation (−100), defining the scale range. HiBiT-IKZF3 MM.1S cells and HiBiT-SALL4 SK-N-DZ cells were started from cryovials into their respective media and dispensed onto compound assay-ready-plates at either 3k (SALL4) or 20k (Aiolos) cells/well using a multidrop combi. Plates were subsequently spun for 1 min at 300×*g* and incubated for 6 h at 37 °C, 5% CO_2 in a humidified incubator. HiBiT Lytic Detection Reagents (Promega) was prepared according to manufacturer's instructions, and 5 μL/well of the lytic detection mix was added to each plate using a multidrop combi. Plates were spun for 1 min at 300×*g*, placed on an orbital shaker at 300 rpm for 30 min before reading luminescence on an Envision-1 plate reader according to the manufacturer's instructions.

HiBiT-BRD4 assay was performed as described previously[40,60]. Briefly, on each screening occasion, a cryo-stock was reconstituted in Opti-MEM I media (Gibco 51985-026) containing 2% FBS (Gibco 10270). 5K cells/well were dispensed into a 384-well plate, and compounds were dispensed on top of the cells with an Echo 655 acoustic dispenser system (Beckman), generating a 10-point, half-log dose response. DMSO and dBET6[61] at 1 μM were used as neutral and 100% inhibition control, respectively. Assay plates were incubated for 5 h at 37 °C, 5% CO_2 in a humidified incubator. HiBiT detection was performed as described above.

Data analysis

Raw signals were analyzed in Genedata Screener using 'Neutral Controls minus Inhibitors' method, and dose-response curves were drawn using the 'Smart Fit' condensing method to calculate DC50 values. Compounds were accepted as active when ≥30% response was observed.

For all experiments described in this manuscript, the investigators were blinded to group allocation during data collection and analysis. Chemical synthesis and biochemical experiments are detailed in the Supplemental Information.

Reporting summary

Further information on research design is available in the Nature Portfolio Reporting Summary linked to this article.

Data availability

The data generated in this study is available in Supplementary Information, as well as from the corresponding authors. Proteomics data have been deposited in the Centre for Computational Mass Spectrometry under the accession number MassIVE MSV000099766. Crystal structure of humanised cereblon from Magnetospirillum gryphiswaldense bound by compound **2** is available in PDB (Protein Data Bank) under the PDB ID 9GJQ. Source data are provided with this paper as a Source Data file. Source data are provided with this paper.

Code availability

The code used to develop the model/perform the analyses, and generate results in this study is publicly available (https://doi.org/10.1093/bioadv/vbab041) and (https://bioconductor.org/packages/release/bioc/html/limma.html) under [MIT, CC-BY 4.0; University of Melbourne, GPL]. The specific version of the code associated with this publication is available as Supplementary Data 6.

References

1. Lenz, W. A short history of thalidomide embryopathy. *Teratology* **38**, 203–215 (1988).
2. Vargesson, N. Thalidomide-induced teratogenesis: history and mechanisms. *Birth Defects Res. C Embryo Today* **105**, 140–156 (2015).
3. Moreau, P. et al. Multiple myeloma: ESMO Clinical Practice Guidelines for diagnosis, treatment and follow-up. *Ann. Oncol.* **28**, iv52–iv61 (2017).
4. Matyskiela, M. E. et al. SALL4 mediates teratogenicity as a thalidomide-dependent cereblon substrate. *Nat. Chem. Biol.* **14**, 981–987 (2018).
5. Donovan, K. A. et al. Thalidomide promotes degradation of SALL4, a transcription factor implicated in Duane Radial Ray syndrome. *Elife* **7**, eLife.38430 (2018).
6. Ito, T. et al. Identification of a primary target of thalidomide teratogenicity. *Science* **327**, 1345–1350 (2010).
7. Kohlhase, J. et al. Mutations at the SALL4 locus on chromosome 20 result in a range of clinically overlapping phenotypes, including Okihiro syndrome, Holt-Oram syndrome, acro-renal-ocular syndrome, and patients previously reported to represent thalidomide embryopathy. *J. Med. Genet.* **40**, 473–478 (2003).
8. Koshiba-Takeuchi, K. et al. Cooperative and antagonistic interactions between Sall4 and Tbx5 pattern the mouse limb and heart. *Nat. Genet.* **38**, 175–183 (2006).
9. Kronke, J. et al. Lenalidomide causes selective degradation of IKZF1 and IKZF3 in multiple myeloma cells. *Science* **343**, 301–305 (2014).
10. Lu, G. et al. The myeloma drug lenalidomide promotes the cereblon-dependent destruction of Ikaros proteins. *Science* **343**, 305–309 (2014).
11. Sievers, Q. L. et al. Defining the human C2H2 zinc finger degrome targeted by thalidomide analogs through CRBN. *Science* **362**, eaat0572 (2018).
12. Cowan, A. D. & Ciulli, A. Driving E3 ligase substrate specificity for targeted protein degradation: lessons from nature and the laboratory. *Annu. Rev. Biochem.* **91**, 295–319 (2022).
13. Bekes, M., Langley, D. R. & Crews, C. M. PROTAC targeted protein degraders: the past is prologue. *Nat. Rev. Drug Discov.* **21**, 181–200 (2022).
14. Wu, T. et al. Targeted protein degradation as a powerful research tool in basic biology and drug target discovery. *Nat. Struct. Mol. Biol.* **27**, 605–614 (2020).
15. Scott, J., Michaelides, I. & Schade, M. Property-based optimisation of PROTACs. *RSC Med. Chem.* https://doi.org/10.1039/D4MD00769G (2024).
16. Lipinski, C. A., Lombardo, F., Dominy, B. W. & Feeney, P. J. Experimental and computational approaches to estimate solubility and permeability in drug discovery and development settings. *Adv. Drug Deliv. Rev.* **46**, 3–26 (2001).
17. Apprato, G. et al. Exploring the chemical space of orally bioavailable PROTACs. *Drug Discov. Today* **29**, 103917 (2024).
18. Yang, W., Saboo, S., Zhou, L., Askin, S. & Bak, A. Early evaluation of opportunities in oral delivery of PROTACs to overcome their molecular challenges. *Drug Discov. Today* **29**, 103865 (2024).
19. Churcher, I. Protac-induced protein degradation in drug discovery: breaking the rules or just making new ones?. *J. Med. Chem.* **61**, 444–452 (2018).
20. Moreau, K. et al. Proteolysis-targeting chimeras in drug development: a safety perspective. *Br. J. Pharmacol.* **177**, 1709–1718 (2020).
21. Demichev, V., Messner, C. B., Vernardis, S. I., Lilley, K. S. & Ralser, M. DIA-NN: neural networks and interference correction enable deep proteome coverage in high throughput. *Nat. Methods* **17**, 41–44 (2020).
22. Messner, C. B. et al. Ultra-fast proteomics with scanning SWATH. *Nat. Biotechnol.* **39**, 846–854 (2021).

23. Teng, M. et al. Development of PDE6D and CK1alpha degraders through chemical derivatization of FPFT-2216. *J. Med. Chem.* **65**, 747–756 (2022).
24. Matyskiela, M. E. et al. A novel cereblon modulator recruits GSPT1 to the CRL4(CRBN) ubiquitin ligase. *Nature* **535**, 252–257 (2016).
25. Powell, C. E. et al. Chemically induced degradation of anaplastic lymphoma kinase (ALK). *J. Med. Chem.* **61**, 4249–4255 (2018).
26. Dahut, W. L. et al. Phase I study of oral lenalidomide in patients with refractory metastatic cancer. *J. Clin. Pharmacol.* **49**, 650–660 (2009).
27. Pal, R. et al. Immunomodulatory derivatives induce PU.1 down-regulation, myeloid maturation arrest, and neutropenia. *Blood* **115**, 605–614 (2010).
28. Fink, E. C. et al. Crbn (I391V) is sufficient to confer in vivo sensitivity to thalidomide and its derivatives in mice. *Blood* **132**, 1535–1544 (2018).
29. Li, S. et al. IMiD compounds affect CD34(+) cell fate and maturation via CRBN-induced IKZF1 degradation. *Blood Adv.* **2**, 492–504 (2018).
30. Reist, M., Carrupt, P. A., Francotte, E. & Testa, B. Chiral inversion and hydrolysis of thalidomide: mechanisms and catalysis by bases and serum albumin, and chiral stability of teratogenic metabolites. *Chem. Res. Toxicol.* **11**, 1521–1528 (1998).
31. Hartmann, M. D. et al. Thalidomide mimics uridine binding to an aromatic cage in cereblon. *J. Struct. Biol.* **188**, 225–232 (2014).
32. Borjesson, U. et al. Synthesis of heterocyclic substituted pyrimidine anticancer agents. WO2022069520 (2022).
33. Jarusiewicz, J. A. et al. Phenyl dihydrouracil: an alternative cereblon binder for PROTAC design. *ACS Med. Chem. Lett.* **14**, 141–145 (2023).
34. Xie, H. et al. Development of substituted phenyl dihydrouracil as the novel achiral cereblon ligands for targeted protein degradation. *J. Med. Chem.* **66**, 2904–2917 (2023).
35. Freeman-Cook, K. D., Hoffman, R. L. & Johnson, T. W. Lipophilic efficiency: the most important efficiency metric in medicinal chemistry. *Future Med. Chem.* **5**, 113–115 (2013).
36. Hopkins, A. L., Groom, C. R. & Alex, A. Ligand efficiency: a useful metric for lead selection. *Drug Discov. Today* **9**, 430–431 (2004).
37. Astles, P. & Scott, J. Preparation of bifunctional PROTAC degraders of androgen receptors. WO2024189488 (2024).
38. Packer, M. J. et al. Preparation of nitrogen-containing heterocyclic compounds and their use in treating cancer. WO2023139199 (2023).
39. Filippakopoulos, P. et al. Selective inhibition of BET bromodomains. *Nature* **468**, 1067–1073 (2010).
40. Plesniak, M. P. et al. Rapid PROTAC discovery platform: nanomole-scale array synthesis and direct screening of reaction mixtures. *ACS Med. Chem. Lett.* **14**, 1882–1890 (2023).
41. Lu, J. et al. Hijacking the E3 ubiquitin ligase cereblon to efficiently target BRD4. *Chem. Biol.* **22**, 755–763 (2015).
42. Delmore, J. E. et al. BET bromodomain inhibition as a therapeutic strategy to target c-Myc. *Cell* **146**, 904–917 (2011).
43. Oleinikovas, V., Gainza, P., Ryckmans, T., Fasching, B. & Thomä, N. H. From thalidomide to rational molecular glue design for targeted protein degradation. *Annu. Rev. Pharmacol. Toxicol.* **64**, 291–312 (2024).
44. Liu, A. et al. Immunomodulatory drugs downregulate IKZF1 leading to expansion of hematopoietic progenitors with concomitant block of megakaryocytic maturation. *Haematologica* **103**, 1688–1697 (2018).
45. Campbell, R. A. et al. IFITM3 regulates fibrinogen endocytosis and platelet reactivity in nonviral sepsis. *J. Clin. Invest.* **132**, e153014 (2022).
46. Bennett, C. L. et al. Thalidomide- and lenalidomide-associated thromboembolism among patients with cancer. *JAMA* **296**, 2558–2560 (2006).
47. Zonder, J. A. et al. Thrombotic complications in patients with newly diagnosed multiple myeloma treated with lenalidomide and dexamethasone: benefit of aspirin prophylaxis. *Blood* **108**, 403 (2006).
48. Ichikawa, S. et al. The cyclimids: degron-inspired cereblon binders for targeted protein degradation. *Cell Chem. Biol.* **31**, 1162–1175 e1110 (2024).
49. Nguyen, T. M. et al. Proteolysis-targeting chimeras with reduced off-targets. *Nat. Chem.* **16**, 218–228 (2024).
50. Wu, H. et al. Development of multifunctional histone deacetylase 6 degraders with potent antimyeloma activity. *J. Med. Chem.* **62**, 7042–7057 (2019).
51. Brennan, P. J. et al. Orthogonal IMiD-degron pairs induce selective protein degradation in cells. ACS Chem. Biol. 20, 2025–2843 (2025).
52. Szewczyk, S. M., Verma, I., Edwards, J. T., Weiss, D. R. & Chekler, E. L. P. Trends in neosubstrate degradation by cereblon-based molecular glues and the development of novel multiparameter optimization scores. *J. Med. Chem.* **67**, 1327–1335 (2024).
53. Axford, J. et al. Preparation of dihydropyrimidines as glue degraders for the treatment and prevention of diseases mediated by various target proteins. WO2021053555 (2021).
54. Gundry, M. C. et al. Highly efficient genome editing of murine and human hematopoietic progenitor cells by CRISPR/Cas9. *Cell Rep.* **17**, 1453–1461 (2016).
55. DeWitt, M. A. et al. Selection-free genome editing of the sickle mutation in human adult hematopoietic stem/progenitor cells. *Sci. Transl. Med.* **8**, 360ra134 (2016).
56. Bak, R. O., Dever, D. P. & Porteus, M. H. CRISPR/Cas9 genome editing in human hematopoietic stem cells. *Nat. Protoc.* **13**, 358–376 (2018).
57. Skowronek, P. et al. Rapid and in-depth coverage of the (phospho-) proteome with deep libraries and optimal window design for dia-PASEF. *Mol. Cell Proteomics* **21**, 100279 (2022).
58. Demichev, V. et al. dia-PASEF data analysis using FragPipe and DIA-NN for deep proteomics of low sample amounts. *Nat. Commun.* **13**, 3944 (2022).
59. Quast, J. P., Schuster, D. & Picotti, P. protti: an R package for comprehensive data analysis of peptide- and protein-centric bottom-up proteomics data. *Bioinform. Adv.* **2**, vbab041 (2022).
60. Lucas, S. C. C. et al. Optimization of potent ligands for the E3 ligase DCAF15 and evaluation of their use in heterobifunctional degraders. *J. Med. Chem.* **67**, 5538–5566 (2024).
61. Nowak, R. P. et al. Plasticity in binding confers selectivity in ligand-induced protein degradation. *Nat. Chem. Biol.* **14**, 706–714 (2018).

Acknowledgements

We thank the compound management team, the global cell bank, and the animal facility team at AstraZeneca for their support with experiments in the manuscript. We thank David Longmire for assistance with NMR spectroscopy.

Author contributions

M.C.R.-B., I.N.M. and K.M. designed the study, performed experiments and wrote the manuscript. J.C.K., T.A., A.A., S.B., F.G., L.R., U.B., G.W.C., G.M.D.D., F.E., N.G., N.B., A.G., C.G., G.M.H., A.H., C.K., P.K., E.L., X.L., R.M., K.M.-B., E.M., P.N., J.O., F.P., C.Pa., M.P., C.Ph., I.P., A.P., T.R., S.R., J.R., I.S., J.W., X.Z. and I.N.M. designed and performed the experiments.

Competing interests

The authors declare the following competing interests: all the authors are or have been employed by AstraZeneca or Pharmaron. The synthesis of CRBN ligands and their associated CRBN binding data for compounds **2, 3, 4, 5, 6, 8** and **12** are reported in patent number: PCT/EP2021/076752 (WO2022069520); status of application: national phase applications pending; patent applicant: Astrazeneca AB; Inventors:

Borjesson, Ulf; Perry, Matthew William Dampier; Grebner, Christoph; Michaelides, Iacovos Neal; Hayhow, Thomas George Christopher; Kettle, Jason Grant; Collie, Gavin William; Storer, Robert Ian; Bagal, Sharanjeet Kaur; Fallan, Charlene.

Additional information

Supplementary information The online version contains supplementary material available at https://doi.org/10.1038/s41467-026-70663-1.

Correspondence and requests for materials should be addressed to Iacovos N. Michaelides or Kevin Moreau.

Peer review information *Nature Communications* thanks Alison Leed and the other anonymous reviewer(s) for their contribution to the peer review of this work. A peer review file is available.

[1]Safety Sciences, Clinical Pharmacology & Safety Sciences, R&D, AstraZeneca, Cambridge, UK. [2]Assays, Profiling & Cell Sciences, Discovery Sciences, R&D, AstraZeneca, Boston, MA, USA. [3]Protein, structure and biophysics, Discovery Sciences, R&D, AstraZeneca, Cambridge, UK. [4]Protein, structure and biophysics, Discovery Sciences, R&D, AstraZeneca, Gothenburg, Sweden. [5]Hit Discovery, Discovery Sciences, R&D, AstraZeneca, Gothenburg, Sweden. [6]Assays, Profiling & Cell Sciences, Discovery Sciences, R&D, AstraZeneca, Cambridge, UK. [7]Assays, Profiling & Cell Sciences, Discovery Sciences, R&D, AstraZeneca, Gothenburg, Sweden. [8]Data Sciences & Quantitative Biology, Discovery Sciences, R&D, AstraZeneca, Boston, MA, USA. [9]Integrated Bioanalysis, Clinical Pharmacology & Safety Sciences, R&D, AstraZeneca, Cambridge, UK. [10]Pharmaron Beijing Co., Ltd, 100176 Beijing, People's Republic of China. [11]Animal Science & Technologies, Clinical Pharmacology & Safety Sciences, R&D, AstraZeneca, Cambridge, UK. [12]Centre for Genomics Research, Discovery Sciences, BioPharmaceuticals R&D, AstraZeneca, Gothenburg, Sweden. [13]Medicinal Chemistry, Research and Early Development, Respiratory & Immunology, BioPharmaceuicals R&D, AstraZeneca, Gothenburg, Sweden. [14]DMPK, Oncology R&D, AstraZeneca, Cambridge, UK. [15]Hit Discovery, Discovery Sciences, R&D, AstraZeneca, Cambridge, UK. ✉e-mail: iacovos.michaelides@astrazeneca.com; kevin.moreau@astrazeneca.com